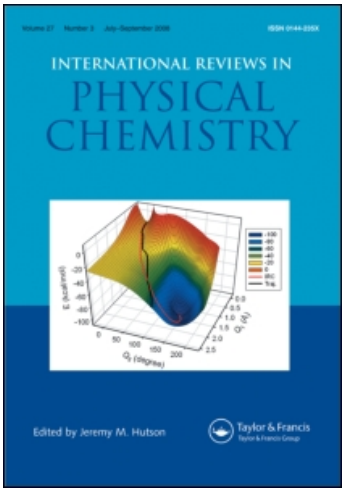

International Reviews in Physical Chemistry
Publication details, including instructions for authors and subscription information:
http://www.informaworld.com/smpp/title~content=t713724383

Molecular dynamic photoelectron spectroscopy using resonant multiphoton ionization for photophysics and photochemistry

Katsumi Kimura[a]
[a] Institute for Molecular Science, Okazaki, Japan

To cite this Article Kimura, Katsumi(1987) 'Molecular dynamic photoelectron spectroscopy using resonant multiphoton ionization for photophysics and photochemistry', International Reviews in Physical Chemistry, 6: 3, 195 — 226
To link to this Article: DOI: 10.1080/01442358709353405
URL: http://dx.doi.org/10.1080/01442358709353405

INTERNATIONAL REVIEWS IN PHYSICAL CHEMISTRY, 1987, VOL. 6, NO. 3, 195–226

Molecular dynamic photoelectron spectroscopy using resonant multiphoton ionization for photophysics and photochemistry

by KATSUMI KIMURA
Institute for Molecular Science, Okazaki, 444 Japan

Photoelectron kinetic-energy spectra of resonant multiphoton ionization of gaseous molecules are regarded as 'photoelectron spectra of the resonant intermediate excited states'. Therefore, such a technique using resonant multiphoton ionization or stepwise ionization with a tunable pulse U.V./visible laser makes it possible to observe excited-state photoelectron spectra for various molecules and molecular complexes in the gas phase. Molecular nonradiative electronic states for which direct observation is difficult by fluorescence spectroscopy can be studied by this technique. It is possible to study not only static but also dynamic aspects of various molecular excited states from the point of view of photoelectron spectroscopy. In this sense, such photoelectron spectroscopy may be called 'dynamic photoelectron spectroscopy'. This is in striking contrast to VUV photoelectron spectroscopy which is mostly concerned with static aspects of ground-state molecules, although information on the dynamics of ionization processes can be obtained. Molecular dynamic photoelectron spectroscopy will be fruitful especially for studying dynamic aspects of molecular excited states from the photophysical and photochemical points of view. The present article is concerned mainly with dynamic photoelectron spectroscopy and its application to molecular processes such as photodissociation, autoionization, and intramolecular relaxation.

1. Introduction

When molecules in the gas phase are excited to specific excited electronic states by laser radiation in the U.V./visible region, resonant ionization is remarkably enhanced and photoelectrons are ejected by a total of two or more photons. Such multiphoton ionization (often abbreviated as MPI) provides a new type of sensitive detection and spectroscopy for excited electronic states in the field of molecular science. Resonant multiphoton ionization (or stepwise ionization) of molecules has been studied mainly by three techniques; (1) ion-current measurements as a function of laser wavelength, (2) mass spectroscopic measurements as a function of the mass of positive ions, and (3) photoelectron spectroscopic measurements as a function of electron kinetic energy. This situation is similar to that in one-photon VUV studies of ground-state molecules.

Concerning MPI photoelectron spectroscopy, there is only one comprehensive review article covering the studies published up to 1983 (Kimura 1985). For MPI ion-current and mass spectroscopic studies of molecules, there are several comprehensive review articles (Johnson 1980 a, b, Robin 1980, Johnson and Otis 1981, Antonov and Letokhov 1981, Lichtin *et al.* 1981, Schlag and Neusser 1983, Parker 1983, Bekow and Letokhov 1983, Gobeli *et al.* 1984). A number of experimental and theoretical studies on MPI processes have been summarized in recent books (Letokhov 1983, Lin *et al.* 1984, Lambropoulos and Smith 1984).

A photoelectron spectroscopic technique combined with a pulsed U.V./visible laser makes it possible to perform photoelectron kinetic-energy measurements for short-lived excited states. This technique has been developed by Kimura and co-workers

(Achiba *et al.* 1980, 1981 a, b, c, 1982), independently of several other groups, namely by Compton (Compton *et al.* 1980, Miller and Compton 1981 a, b), Reilly (Meek *et al.* 1980, 1982), Agostini *et al.* (1981), Robin (Fisanik *et al.* 1981), Van der Wiel (Kruit *et al.* 1981, Kimman *et al.* 1982), Colson (Glownia *et al.* 1982, White *et al.* 1982), Zare (Anderson *et al.* 1982), and by Dehmer (Pratt *et al.* 1983 a, b).

Photoelectron angular-distribution measurements for excited states can be carried out with a U.V./visible laser technique, but only a few compounds have so far been studied, namely, NH_3 and NO (Achiba *et al.* 1983 a, 1985), H_2 (Anderson *et al.* 1984), and NO (White *et al.* 1984). For excited atoms, however, a considerable number of papers have been published on their photoelectron angular distribution (for example, Edelstein *et al.* 1974, Berry 1976, Hansen *et al.* 1980, Kaminski *et al.* 1980, Feldmann and Welge 1982, Kruit and Read 1983, Sato *et al.* 1984 a, Compton *et al.* 1984, Pratt *et al.* 1985 a).

An energy level diagram relevant to MPI ion-current and photoelectron spectra is schematically shown in figure 1. When the laser wavelength is scanned in the U.V./visible region, one may obtain MPI ion-current peaks corresponding to resonant excited states (vibrationally and rotationally resolved). Such an MPI ion-current spectrum provides information about the energy levels of resonant excited states, as in optical absorption spectroscopy. Excited states such as one-photon-forbidden two-photon-allowed transitions are also observable by an MPI ion-current spectroscopic technique.

Photoelectron kinetic-energy measurements at each MPI ion-current peak provide photoelectron spectra of resonant excited states. Such a photoelectron spectrum is schematically shown in the upper part in figure 1. Primary information deduced from an excited-state photoelectron spectrum relates to the ionic states produced by the optical selection rule from the resonant excited states. In other words, the photoelectron kinetic-energy spectrum thus obtained at each MPI ion-current peak is

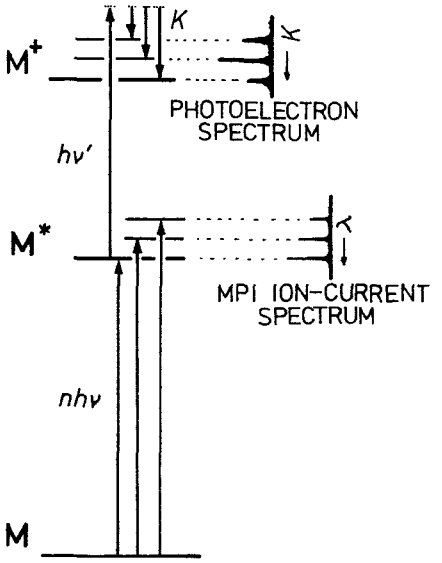

Figure 1. Schematic energy level diagram of a molecule, relevant to $(n+1)$-type resonant multiphoton ionization. MPI ion-current and photoelectron spectra are shown schematically.

regarded as a photoelectron spectrum inherent in the resonant intermediate state. In this sense, an MPI photoelectron spectrum gives a fingerprint identification for excited states.

For example, a photoelectron spectrum obtained by one-photon resonant two-photon ionization through the $v'=0$ vibrational level of the Rydberg A $^2\Sigma^+$ state of NO shows only a single vibrational peak due to the $v^+=0$ level of the $NO^+(X)$ ion (Achiba and Kimura 1984 b), because the NO bond distance of this Rydberg excited state is almost the same as that of the ionic state. However, a HeI photoelectron spectrum available for NO shows the first ionization band that consists of several vibrational peaks (Turner *et al.* 1970). Comparison of these two kinds of photoelectron spectra demonstrates a dramatic difference in spectral pattern. In general, an excited-state photoelectron spectrum essentially differs from a VUV ground-state photoelectron spectrum, reflecting more or less a difference in molecular geometry between the excited state and the ground state. Ionization potential data of VUV photoelectron spectroscopy have been compiled in handbooks (Siegbahn *et al.* 1974, Kimura *et al.* 1981).

The photoelectron spectrum of a molecular excited electronic state is similar in quality of information to the corresponding fluorescence spectrum, when fluorescence is emitted from that state. However, as far as transition probability is concerned, the two kinds of electronic processes are quite different. Ionization is always allowed for a one-electron transition for any excited state, and the ionization transition probabilities are of the same order of magnitude. However, fluorescence transition probabilities vary by several orders of magnitude. Observations of molecular fluorescence spectra in the gas phase are very limited. Different electronic states of ions can be produced as the final states in ionization by an appropriate laser. This situation also differs from that in molecular fluorescence spectroscopy.

Recently, excited-state photoelectron spectroscopy has been further extended in this Institute to study the dynamic behaviour of molecular excited states, and various results demonstrating its versatility have been accumulated to a considerable extent, as described in the present article. When a nanosecond laser is used, it is possible to study dynamic behaviour of excited states in the nanosecond domain.

For the reasons given above, it seems appropriate to review the present situation of molecular dynamic photoelectron spectroscopy. The purpose of the present article is to outline the study of dynamic photoelectron spectroscopy, as well as to describe in some detail its several recent applications. Characteristics and advantages of this method are also summarized.

2. General features and characteristics

Excited-state photoelectron spectroscopy has the potential for observing the dynamic behaviour of excited states. Since a molecular excited electronic state may undergo photophysical or photochemical phenomena, this photoelectron spectroscopy should provide new information about the photophysics and photochemistry of electronically excited molecules in the gas phase. The time evolution of the excited state can be studied in terms of the change of the photoelectron spectral pattern under various laser conditions. Because of this capability of observing the time evolution of the excited states, excited-state photoelectron spectroscopy may be called 'dynamic photoelectron spectroscopy'.

By combining a pulse laser system with a time-of-flight photoelectron detection system, it is possible to carry out photoelectron spectroscopic measurements for

excited states. Nanosecond U.V./visible lasers have been used for this purpose. The experimental technique of photoelectron energy analysis is well established, as described in a previous review (Kimura 1985). Under mild laser conditions, resonant multiphoton ionization may be regarded as a stepwise process, as shown in figure 1. If two lasers are used for this purpose, the photon energy of the second laser can be changed, while the first laser is kept at a constant wavelength.

2.1. *Resonant multiphoton ionization*

When the wavelength of an appropriate laser in the U.V./visible region is tuned to each optically allowed transition of an excited state of a molecule in the gas phase, resonant multiphoton ionization takes place by ejecting photoelectrons, and hence the ion current is remarkably enhanced. The stepwise process of resonant multiphoton ionization with a single laser (ν_1) is described by

$$M \xrightarrow{nh\nu_1} M^* \xrightarrow{mh\nu_1} (M^+)_i + (e^-)_i \tag{1}$$

where M means the ground state, M* a resonant intermediate state, $(M^+)_i$ the ionic state i of the molecule, and $(e^-)_i$ the photoelectron ejected with the kinetic energy which corresponds to the ionic state i. Such a stepwise process commonly proceeds during a single laser pulse.

If another appropriate laser (ν_2) is used along with the first laser (ν_1), then the resonant excited state produced by the first laser is also ionized by the second laser to eject photoelectrons with different kinetic energies:

$$M^* \xrightarrow{mh\nu_2} (M^+)_i + (e^-)_i \tag{2}$$

The advantage of using two lasers is that the wavelength of the second laser can be selected independently of the first one. By photoelectron energy analysis, process (2) can be distinguished from process (1). There is a possibility of accidental resonant ionization by the second laser alone.

When a molecule is excited by m photons to its specific resonant excited state and subsequently ionized by n photons, this ionization process is called 'm-photon resonant $(n+m)$-photon ionization' and often abbreviated as '$(m+n)$ resonant ionization'. The two processes expressed by $(2+1)$ and $(1+2)$ at the same laser frequency differ in the resonant excited state. If an accidental double resonance takes place, the process may be expressed as $(1+1+1)$.

The ionization process by photon absorption is an allowed electronic transition. In principle, ionization at any excited electronic state takes place in competition with other deactivation processes such as relaxation or dissociation. This situation is shown schematically in figure 2. The rate of ionization at a specific excited state is given by the product of the laser intensity I (photons/cm^2 s) and the ionization cross-section σ_i (cm^2); namely

$$k_i = I\sigma_i \tag{3}$$

The ion yield Y_i is given by

$$Y_i = k_i/(k_i + k_r) \tag{4}$$

where k_r is the rate of deactivation at the excited state.

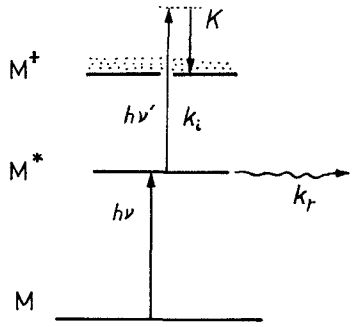

Figure 2. Schematic energy diagram, showing that the ionization process competes with an intramolecular relaxation process in the resonant excited state.

The ionization rate under nanosecond laser conditions (10 ns, 1 mJ) has been estimated as follows (Achiba and Kimura 1984 b). When laser radiation with a cross-section of 1 cm^2 and an energy of 1 mJ (10^{15} photons/pulse) is focused by a lens on the area of an order of 10^{-6} cm^2, then the photon intensity during the 10-ns laser pulse density is given by $I \approx 10^{29}\,cm^{-2}\,s^{-1}$. If the ionization cross-section of the resonant excited state is assumed to be similar to that of the ground state, namely, 10^{-17}–10^{-18} cm^2, then the rate of ionization is estimated to be $k_i = 10^{11}$–$10^{12}\,s^{-1}$.

Under such laser conditions, for example, the NH_3 molecule at the Rydberg A $v' = 0, 1$ levels can be ionized in competition with its rapid picosecond predissociation. Their lifetimes are known to be 10^{-12}–10^{-13} s (Douglas 1963, Hackett *et al.* 1977). According to an MPI ion-current study (Glownia *et al.* 1980), the picosecond predissociation of the Rydberg A state ($v' = 0$ and 1) is responsible for the relatively weak MPI signal and is competitive with the photoionization process. An MPI ion-current spectrum observed for jet-cooled NH_3 under the above-mentioned laser conditions is shown in figure 3, indicating that the two bands assigned to the Rydberg A $v' = 0$ and 1 levels are considerably broad compared with other bands. The band width of the A $v' = 1$ band in figure 3 is about 60 cm^{-1}, yielding a lifetime of about 8×10^{-13} s,

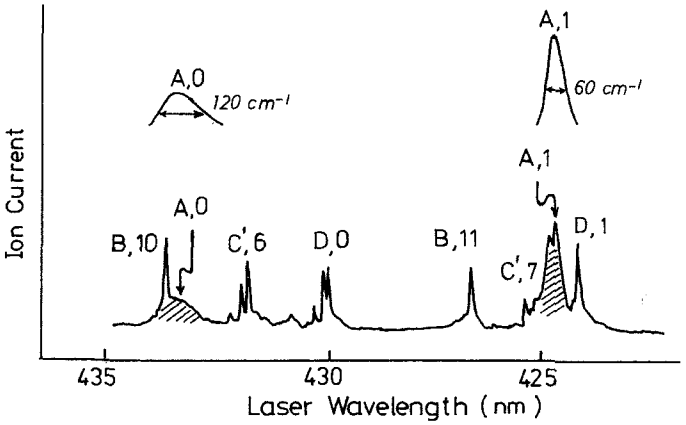

Figure 3. The MPI ion-current spectrum of ammonia, showing two broad bands associated with rapid predissociation at the Rydberg A $v' = 0, 1$ levels (Achiba and Kimura 1984 b).

which is consistent with the available value (10^{-12}–10^{-13} s). Therefore it should be emphasized that, in spite of its picosecond predissociation, an MPI ion-current peak due to the NH_3 A $v'=1$ state is observable by a nanosecond laser. Consequently, photoelectron spectroscopic detection for the NH_3 Rydberg A state is possible under such laser irradiating conditions.

2.2. *MPI ion-content spectroscopy*

An MPI ion-current spectrum, obtained as a function of laser wavelengths in the U.V./visible region, consists in general of many resonance peaks which correspond to resonant excited states (see figure 1). Such an ion-current spectrum is often simply called 'MPI spectrum'. In the present paper, however, this will be called 'MPI ion-current spectrum' to distinguish it from 'MPI photoelectron spectrum'.

An MPI ion-current spectrum containing various transitions is observable with the resolution of the tunable laser, so that it often shows a vibrationally and rotationally resolved structure. Therefore it is possible to perform high-resolution spectroscopy for excited states of molecules by means of an MPI ion-current spectroscopic technique (Johnson 1980 a, b). Assignment of resonant excited states from an MPI ion-current spectrum does not require a knowledge of the ionic states which are produced in the resonant multiphoton process studied. This is the most important feature of MPI ion-current spectroscopy. In order to identify the ionic states of parent ions produced, however, it is necessary to carry out photoelectron kinetic-energy analysis.

2.3. *Excited-state photoelectron spectroscopy*

From an MPI ion-current spectrum, we can determine the laser wavelengths at which resonant ionizations take place and hence at which photoelectrons are efficiently ejected. Therefore, it is necessary to measure an MPI ion-current spectrum prior to photoelectron measurements. Photoelectron kinetic-energy measurements are then carried out at individual MPI ion-current peaks.

The number of photons absorbed in the overall ionization process can easily be found from photoelectron energies. This is the most direct method of determining the photon number in MPI processes. Photoelectron energy distribution is governed by many factors which include the optical selection rules and Franck–Condon factors. Many photoelectron studies of resonant multiphoton ionization indicate that the photoelectron vibrational structure can be interpreted in terms of Franck–Condon factors between the resonant excited state and the ionic state. One of the most important features of dynamic photoelectron spectroscopy is that the detection of a photoelectron signal is possible even for a nonradiative electronic state.

If two or more photons are absorbed in the second ionization process, there might be a possibility of an accidental resonance at a higher excited state. If such an accidental resonance occurs, the resulting photoelectron spectrum reflects the upper state of accidental resonance rather than the initial lower resonant state, and hence the situation would be more complicated. When a visible laser is used, its one-photon energy is often not enough to ionize a molecule from its low-lying excited states. In this case, it is necessary to use another U.V. or far-U.V. laser for one-photon ionization of the excited state, independently of the first-excitation laser. The advantages of two-colour experiments in dynamic photoelectron spectroscopy are the following. (1) The condition of one-photon ionization for a resonant excited state can be realized by using a U.V. or far-U.V. laser as the second laser. Under such experimental conditions, it is possible to avoid accidental resonances. (2) Direct ionization can be distinguished from

autoionization by changing the wavelength of the second laser. (3) Dynamic behaviour of an excited state can be studied most properly by firing the second laser with a delay after the first one.

3. Experimental method

Laser photoelectron experiments are usually carried out in two stages. The first step is to measure MPI ion-current spectra as a function of laser wavelength, and the second is to measure the kinetic energies of pulse photoelectrons at each MPI ion-current peak. The kinetic energies of photoelectrons ejected by laser irradiation in the U.V./visible region are low; that is, in general they are lower than the one-photon energy of the laser. Therefore, energy analysis of pulse slow photoelectrons is required. This is in remarkable contrast to conventional VUV photoelectron spectroscopy, in which photoelectron energies are usually much higher.

3.1. *Apparatus*

The photoelectron apparatus which has been constructed by the author's group is briefly described here (Kimura 1985, Achiba *et al.* 1980, 1981 a, 1982). The whole apparatus consists of (1) a U.V./visible nanosecond laser system which is used for the excitation and ionization of the gas sample, (2) a nozzle beam source which introduces a gas sample intermittently into a vacuum chamber, (3) a main vacuum chamber in which ionization experiments are carried out for ion-current and photoelectron measurements, (4) a time-of-flight (TOF) photoelectron energy analyser, (5) a detection and data acquisition system for ion-current and photoelectron spectra.

A pulsed nozzle injector with an orifice of 0·3–0·7 mm in diameter is used. Its duration is 1 ms, while its repetition rate is 10 Hz. A conical skimmer with a 1 mm aperture is used. The total ion current obtained for each laser shot is converted to a voltage by a fast current amplifier, and then averaged by a boxcar integrator. The output signals from the boxcar are recorded on a strip chart recorder. Photoelectron energies are measured by the TOF drift tube which will be mentioned later. Ion masses are measured with the same TOF analyser as in the photoelectron measurements. In the mass spectrometry mode, ions are accelerated by an electric field imposed by a repeller and an extractor, which are set typically at 5 and 10 volts, respectively. The repeller and extractor are discs of gold-plated brass separated by 30 mm, each with a hole 10 mm in diameter. The ions are then focused by three cylindrical lenses, introduced into the TOF analyser tube.

3.2. *Laser source*

A Nd-YAG-based tunable laser system is used for nanosecond pulse laser radiation in the visible/U.V. region, consisting of a Nd-YAG laser, two dye lasers, and a wavelength extender. The second harmonic (532 nm) of the 1064 nm fundamental, generated by a harmonic generator, pumps appropriate dyes to cover the wavelengths 420–700 nm. The wavelength extender covers the range 216–432 nm by frequency doubling and mixing in KDP and KDP* crystals. An excimer-driven tunable laser system is also used, consisting of an excimer laser with gases ArF (194 nm), KrF (249 nm), XeCl (308 nm), and a dye laser to generate tunable output. Furthermore, a hydrogen Raman shifter is also used to generate the nth anti-Stokes lines (199·8, 204·2, 208·8, 217·8, and 228·7 nm), using the second, third, and fourth harmonics of the 1064 nm Nd-YAG fundamental. Laser radiation is focused by an $f = 10$–25 cm lens onto the ionization region located about 10 nm downstream from the nozzle tip.

3.3. *Photoelectron energy analysis*

A TOF electron analyser is used for photoelectron energy analysis. Photoelectrons travel through a 12–20 cm drift tube to an electron multiplier (Channeltron) located at the terminus of the tube. A laser pulse detected by a fast pindiode, triggers the sweep of a transient recorder (500 MHz/channel, 2 ns/channel) into which the photoelectron signals are fed from the electron multiplier. Signal averaging and data storage are performed by a microcomputer-controlled data acquisition system. Calibration for the photoelectron energy scale is carried out by using available photoelectron energies of, for example, (2 + 1) resonant ionization of NO through its Rydberg A state. Magnetic shielding is especially important for such low-energy photoelectrons.

In general, two types of analysers have been used for electron energy analysis; one is the abovementioned TOF electron analyser, and the other is a spherical electrostatic analyser. A TOF analyser coupled with an electron parallellizer has also been used (Kruit *et al.* 1981, 1982). In this analyser, all electrons with a component of initial velocity in the direction of the detector are parallellized by a diverging magnetic field along the axis of the TOF tube. A 160° spherical sector and a hemispherical analyser were used by Compton *et al.* (1980) and Pratt *et al.* (1983 a, b), respectively.

4. Photodissociation of iron complexes

A molecule irradiated by a laser pulse undergoes two typical types of nonlinear photochemistry: ionization followed by fragmentation, and fragmentation followed by ionization (Gedanken *et al.* 1982). Laser excitation of gaseous metal carbonyl complexes such as $Fe(CO)_5$ in the region of the charge-transfer band around 280 nm produces Fe^+ ions with almost unit efficiency at relatively mild laser fluence (Duncan *et al.* 1979).

Several U.V./visible MPI studies of metal carbonyls and organometallic compounds have indicated sharp MPI ion-current peaks which can be attributed to resonant ionizations of the ground-state metal atoms (Gerrity *et al.* 1980, Leutwyler *et al.* 1980, Engelking 1980). A laser photoelectron study (Nagano *et al.* 1982) has indicated that several prominent MPI peaks of $Fe(CO)_5$ in the visible region 447–466 nm are attributed to three-photon resonant ionizations of the ground-state Fe atoms. Some MPI ion-current peaks due to the first excited states (spin–orbit split) of Fe atoms have also been reported (Engelking 1980, Whetten *et al.* 1983). Furthermore, recent photoelectron spectroscopic studies (Nagano *et al.* 1986 a, b, c) have identified thirteen low-lying electronic states of Fe atoms in the photodissociation of $Fe(CO)_5$.

When many different electronic states of metal atoms are formed in the photodissociation of metal complexes, it is often difficult to determine the electronic states from MPI ion-current spectra alone, since there are a number of possible resonant excited states of the metal atoms. The idea of using photoelectron spectroscopy is to determine the initial electronic states on the basis of the photoelectron energy maxima. This situation is schematically shown in figure 4. In this case it is unnecessary to know resonant intermediate states. In other words, photoelectron spectroscopy makes it possible to determine the initial electronic states of metal atoms without knowing resonant excited states.

Broad bands and background signals appearing in MPI ion-current spectra for iron complexes have been studied by photoelectron energy analysis (Nagano *et al.* 1986 b, c). It is especially difficult to interpret the broad feature and background signals of MPI ion-current spectra without photoelectron energy data. According to the photoelectron spectroscopic studies (Nagano *et al.* 1986 b, c), the broad bands are due

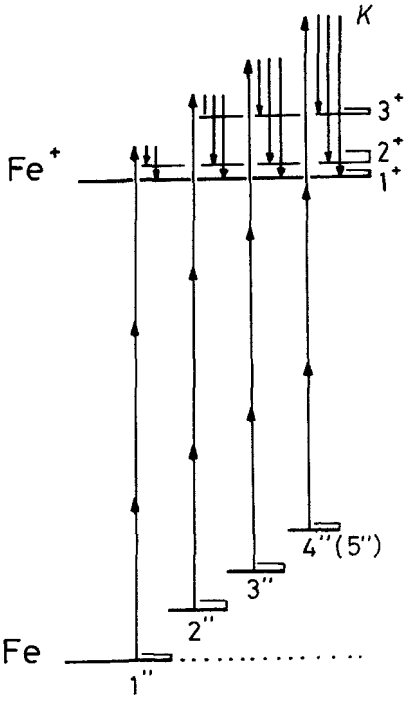

Figure 4. Schematic energy diagram of the Fe atom and Fe^+ ion, showing the principle of photoelectron determination of the initial electronic state.

to congestion of resonant ionizations of higher excited states, and the background signal is due to non-resonant multiphoton ionization of higher excited states. The photoelectron studies reported for the photodissociation of iron complexes are described in some detail in this Section.

4.1. *Photoelectron determination of electronic states*

A typical MPI ion-current spectrum observed for $Fe(CO)_5$ in the laser wavelength 447–450 nm is shown in figure 5, indicating many weak and strong peaks by the numbering $N = 5$–26 (Nagano *et al.* 1986 a). From photoelectron energy analysis, all these peaks have been interpreted in terms of the three-photon resonant ionizations originating from the lowest four electronic states of Fe atoms. (These resonant ionizations correspond to the four processes shown in figure 4.) Several typical photoelectron spectra due to Fe^+ ions are shown in figure 6, produced from the different electronic states of Fe atoms.

The photoelectron energy K in the three-photon ionization of an Fe atom is given by

$$K = 3h\nu - I + E(i'') - E(j^+) \tag{5}$$

where $3h\nu$ is the total photon energy, I is the first ionization potential (7·90 eV), and $E(i'')$ and $E(j^+)$ are the energies of the ith initial neutral electronic state and the jth final ionic state, respectively. In this Section, the electronic terms of Fe and Fe^+ are abbreviated as

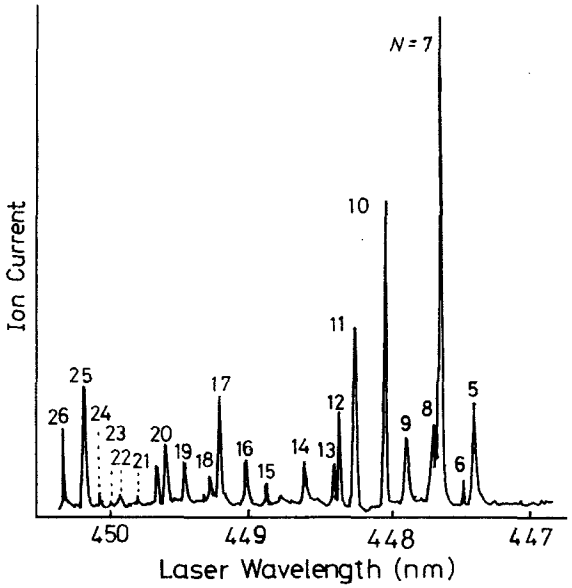

Figure 5. MPI ion-current spectrum of the Fe atom obtained by three-photon ionization (Nagano *et al.* 1986 a). The peaks shown here are indicated by the numbers $N = 5$–26. The electronic states of Fe and Fe^+ are indicated by $i''(1'', 2'', 3'', \ldots)$ and j^+ $(1^+, 2^+, 3^+, \ldots)$.

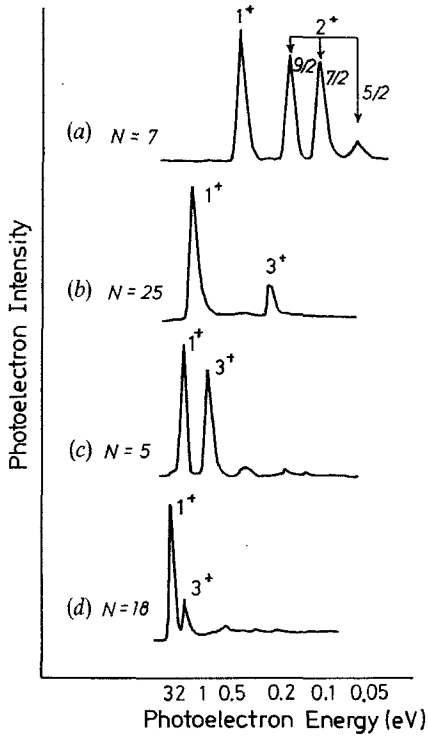

Figure 6. Photoelectron spectra of Fe atoms populated in the ground state and some low-lying excited states (Nagano *et al.* 1986 a), observed at the MPI ion-current peaks $N = 5$, 7, 18, and 25 shown in figure 5.

$i''(1'', 2'', \text{etc.})$ and $j^+(1^+, 2^+, \text{etc.})$, respectively. Formation of the lowest ionic state gives rise to the maximum photoelectron energy which is given by

$$K_{max} = 3h\nu - I + E(i'') \tag{6}$$

since $E(1^+) = 0$. From equation (6), the maximum photoelectron energies for Fe atoms populated at the lowest four electronic states are evaluated to be $K_{max} = 0{\cdot}33$–$0{\cdot}56$, $1{\cdot}19$–$1{\cdot}45$, $1{\cdot}82$–$2{\cdot}05$, and $2{\cdot}51$–$2{\cdot}66$ eV (Nagano *et al.* 1986a). When Fe atoms are produced in many different electronic states, such evaluations of maximum photoelectron energies are helpful for interpreting MPI ion-current peaks.

The four typical photoelectron spectra in figure 6 are briefly explained here. Photoelectron spectrum (*a*), obtained at the ion-current peak $N = 7$, consists of two ionization bands which are due to 1^+ and 2^+ originating from $1''$ (see, process (*a*) in figure 4). The 2^+ band is resolved into a few J levels, since the energy resolution in the region below $K = 0{\cdot}2$ eV is better than 15 meV. The 1^+ band however is not resolved into its J levels, since the resolution is not sufficient in this region. Photoelectron spectra (*b*)–(*d*) observed at $N = 25$, 5, and 18 each show two bands 1^+ and 3^+ originating from $2''$, $3''$, and $4''$ ($5''$), respectively. These spectra correspond to the processes (*b*)–(*d*) shown in figure 4. The 2^+ state is not observed in HeI photoelectron spectra of Fe atoms (Dyke *et al.* 1982). On this point, the resonant multiphoton ionization is in remarkable contrast to VUV one-photon ionization.

The photoelectron analysis has indicated that the lowest four electronic states of Fe atoms are responsible for all the MPI ion-current peaks shown in figure 5. However, resonant intermediate states in the three-photon resonant ionizations of $3''$ and $4''$ ($5''$) have not yet been identified, since there seem to be many unknown excited states in the higher-energy region. In general, such photoelectron spectroscopic determination of the initial electronic states should be useful for studying electronic states of photodissociation products.

4.2. *Ligand effect on electronic-state population*

The photoelectron study (Nagano *et al.* 1986c) has indicated that the electronic-state population of Fe atoms largely depends on the ligand. The MPI ion-current spectra observed for three different iron complexes are shown in figure 7; (*a*) ferrocene $Fe(Cp)_2$, (*b*) iron tris (acetylacetonate) $Fe(Acac)_3$, and (*c*) iron pentacarbonyl $Fe(CO)_5$. All these spectra, showing remarkable differences in spectral pattern, have been attributed to two or three-photon ionization of Fe atoms from photoelectron energy analysis (Nagano *et al.* 1986c). Such remarkable differences in the MPI ion-current spectra are due to significant changes in the electronic-state population of Fe atoms.

The main ion-current peaks in figure 7 are numbered by $N = 1$–11 for convenience. Spectrum (*a*) in figure 7 is the simplest among the three spectra, mainly consisting of four sharp peaks ($N = 3$, 5, 7 and 8), while spectrum (*b*) shows several additional peaks ($N = 1$, 6, 9, 10 and 11) and some weak broad bands. Among these additional peaks, the two peaks $N = 1$ and 11 have been assigned as two-photon resonant ionizations of $3''$; namely, $Fe(a\ ^3F_{2,3}) \rightarrow Fe(x\ ^5D^0_{2,4}) \rightarrow Fe^+$. Spectrum (*c*) showing many broad bands is in striking contrast to spectra (*a*) and (*b*) in figure 7.

Figure 8 shows several typical photoelectron spectra observed at the MPI ion-current peaks $N = 3$, 8, 11, and 2 of figure 7. Spectrum (*a*) in figure 8 indicates two photoelectron bands due to 1^+ and 3^+, whereas spectrum (*b*) shows a band due to 2^+. These photoelectron spectra should reflect the electronic character of resonant excited states. In the case of spectrum (*a*), the electronic configuration of the resonant state

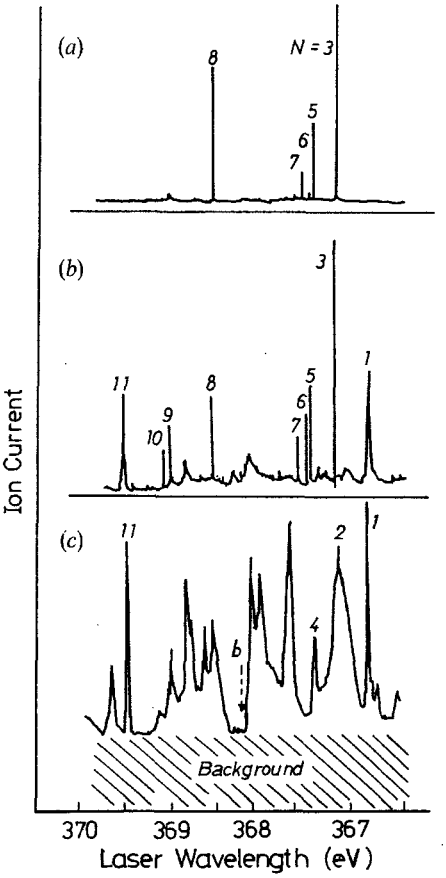

Figure 7. MPI ion-current spectra obtained for three iron complexes (Nagano *et al.* 1986 c); (*a*) ferrocene, $Fe(C_5H_5)_2$; (*b*) iron tris(acetylacetonate, $Fe(Acac)_3$; and (*c*) iron pentacarbonyl, $Fe(CO)_5$. All these spectra originate from Fe atoms populating low-lying electronic states.

allows the formation of 1^+ and 3^+, but inhibits formation of 2^+. The 2^+ state has the electronic configuration $3d^7$, whereas the 1^+ and 3^+ states have the same electronic configuration $3d^64s$. Therefore, photoelectron bands due to 1^+ and 3^+ are often observed as a pair. Spectrum (*c*) in figure 8, obtained at $N = 11$, is an interesting example showing the 1^+ and 2^+ bands. The 2^+ band consists of two spin-orbit-split peaks ($J^+ = 9/2$ and $7/2$), probably due to autoionization. Spectrum (*d*) in figure 8, obtained at $N = 2$, shows broad bands, which are regarded as congestion of several two-photon ionizations originating from 4″–13″ (Nagano *et al.* 1986 c).

Ferrocene and iron pentacarbonyl are two extreme cases, yielding remarkably different patterns in the MPI ion-current spectra. In the one extreme (ferrocene), ground-state Fe atoms are dominantly produced. However, in the other extreme case (iron pentacarbonyl), Fe atoms are broadly populated among the excited states up to 13″. In the middle case, the excited-state population is in between the two extremes, as shown by spectrum (*b*) in figure 7. Many other Fe complexes are probably between the two extremes.

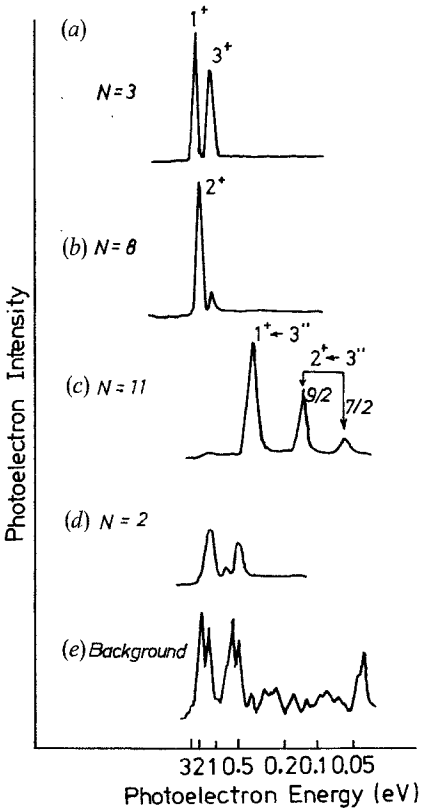

Figure 8. Photoelectron spectra of Fe atoms populated in various low-lying electronic states (Nagano *et al.* 1986 c), obtained at the MPI ion-current peaks $N = 2, 3, 8$, and 11 and also at an MPI background shown by letter b in figure 7 (*c*).

The excitation energy of the parent iron complexes is considered to transfer rapidly to the low-frequency vibrational modes of the ligands. Roughly speaking, the density of the vibrational states increases in the order $Fe(CO)_5$, $Fe(Acac)_3$, $Fe(Cp)_2$. The ratios of the number of the ligand vibrational modes to the number of the metal–ligand stretching modes in the Fe complexes are 5·4 for $Fe(CO)_5$, 22·0 for $Fe(Acac)_3$, and 28·5 for $Fe(Cp)_2$ (Nagano *et al.* 1986 c). These differences probably give rise to the different population of excited-state Fe atoms.

4.3. *Background ion-current*

Significant background signals are observed for some metal carbonyls in the MPI ion-current spectra at a higher laser power (Duncan *et al.* 1979, Engelking 1980, Leutwyler and Even 1981, Gedanken *et al.* 1982, Whetten *et al.* 1983). With increasing laser power, the background ion-current intensity becomes stronger with respect to the sharp peaks. The MPI ion-current spectrum (*c*) in figure 7 shows a significant background signal (the shaded portion). For example, the ion-current intensity indicated by the letter b in figure 7 (*c*) is regarded as a background signal. The photoelectron spectrum obtained at the ion current indicated by the letter b in figure 7 (*c*) is shown by spectrum (*e*) in figure 8. The photoelectron bands appear only below 3·4 eV. This fact indicates that ionization occurs by the minimum number of photons.

In the wavelength region 366–370 nm (figure 7), Fe atoms populated at 3″, 4″,... can be ionized by only two photons. The main components of the photoelectron spectrum (*e*) in figure 8 have been attributed to two-photon ionization of Fe atoms populated among the excited states 4″–11″ (Nagano *et al.* 1986 c).

5. Autoionization of NO

Excitation of a molecule to its superexcited state may lead to autoionization, which produces an ion and a photoelectron, or to dissociation, which produces neutral fragments. If a molecule is excited to one of its superexcited states from a specific lower excited state by double-resonance excitation, then it is possible to study autoionization by the photoelectron intensity distribution.

Several processes of (2 + 1) resonant ionization for the NO molecule are schematically illustrated in figure 9. Processes (*a*), (*c*), and (*d*) in figure 9 show direct ionization, in which the $\Delta v = 0$ transition is dominant. However, processes (*b*) and (*c*) are typical cases, in which $\Delta v = 0$ is forbidden in the sense of the Franck–Condon selection rule. Furthermore, process (*f*) in figure 9 is a typical case, in which direct ionization is electronically forbidden. In other words, one-electron ionization of the non-Rydberg valence-excited B $^2\Pi$ state yields the excited a $^3\Sigma^+$ state of NO^+, that is 6·5 eV above the NO^+ ground state. If a vibrational level of the valence-excited B $^2\Pi$ state is electronically perturbed by Rydberg states, direct ionization should be more or less allowed. The ionization-forbidden regions in processes (*b*), (*e*), and (*f*) are shaded in figure 9. The potential curves relevant to the multiphoton ionization concerned here are schematically shown in figure 10.

Selective excitation is therefore especially advantageous for studying autoionization of molecules. Two-colour experiments are most desirable for this purpose. However, it is possible to study autoionization phenomena with one-colour experiments, as mentioned in this Section. The most important information deduced from photoelectron spectra is the autoionization branching ratio for producing different electronic and vibrational states of ions that cannot be obtained by other methods. The photoelectron branching ratio should provide a clue to the mechanisms of autoionization.

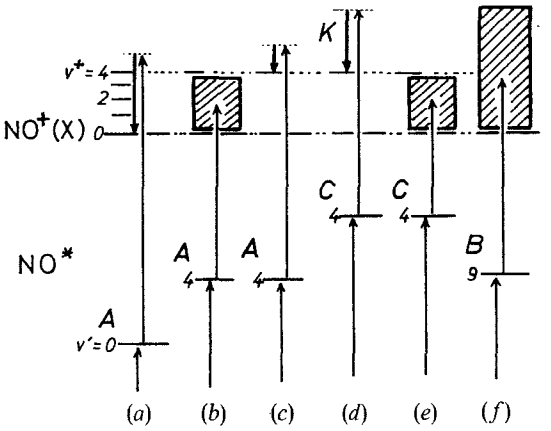

Figure 9. Schematic energy level diagram of the NO molecule, relevant to resonant ionization processes via the Rydberg A ($v' = 0$ and 4), Rydberg C ($v' = 4$), and the non-Rydberg B ($v' = 9$) states. Some forbidden ionization regions are shaded.

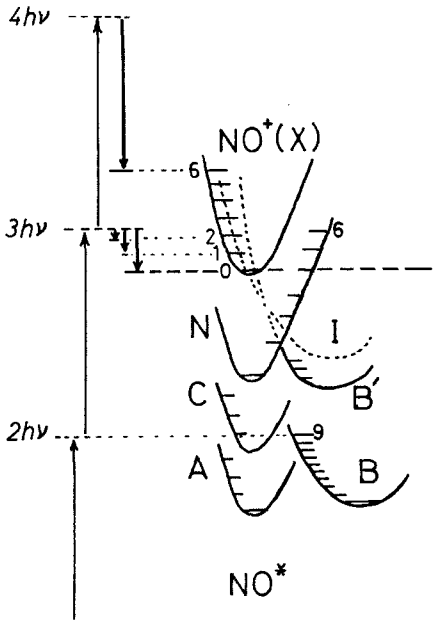

Figure 10. Schematic potential curves relevant to (2+1) resonant ionization of the NO molecule.

Photoelectron spectra for the Rydberg A $^2\Sigma^+$ and C $^2\Pi$ states of NO (Miller and Compton 1981 a) and for the Rydberg F $^2\Delta$ and H $^2\Sigma^+$ states of NO (Achiba *et al.* 1983 a) have been reported. In these studies, $\Delta v=0$ ionization transitions are mainly observed. The $\Delta v=0$ propensity is easily understood, because these Rydberg states are very similar in geometry to the ground-state ion. In order to study autoionization phenomena, it is desirable to distinguish photoelectrons ejected by autoionization from those produced by direct ionization. Distinction between autoionization and direct ionization is possible if one can select a specific excited state from which direct ionization is forbidden. Recently the photoelectron spectra of autoionization for NO have been observed by eliminating the possibility of direct ionization (Achiba *et al.* 1985).

In this Section, photoelectron spectroscopic evidence for autoionization is explained in the following three cases: (1) autoionization by (2+1) resonant excitation via the Rydberg A $^2\Sigma^+$ $v'=4$ level (process (*b*) in figure 9). In this case, the three-photon energy is insufficient to cause $\Delta v=0$ transition. (2) Autoionization by (2+1) resonant excitation via the B $^2\Pi$ $v'=9$ state (process (*f*) in figure 9). In this case, the three-photon energy is insufficient to cause one-electron transition. In other words, two-electron transition is required to produce $NO^+(X)$. (3) Autoionization by (2+1) resonant excitation via the $v'=4$ level of the Rydberg C $^2\Pi$ state (process (*e*) in figure 9). In this case, the three-photon energy is again insufficient to cause the $\Delta v=0$ ionization transition.

5.1. *Autoionization of NO via Rydberg A state*

Concerning direct ionization, photoelectron spectra showing $\Delta v=0$ ionization transitions have been observed for (2+2) resonant ionization of NO via the $v'=0$–3

vibrational levels of the Rydberg A $^2\Sigma^+$ state (Miller and Compton 1981 a, 1982, Kimman *et al.* 1982). When NO is excited to the $v'=4$ level of this Rydberg state by the 374·7 nm two-photon energy, absorption of one more photon exceeds the ionization threshold, but does not reach the $v^+=4$ level of $NO^+(X)$. In other words, the three-photon energy falls in the shaded area shown in figure 9 (*b*).

In spite of the forbidden transition, a weak MPI ion-current spectrum attributable to (2+1) resonant ionization of the A $^2\Sigma^+$ $v'=4$ level can be observed in the laser wavelength region around 374 nm (Achiba and Kimura 1984 b). Figure 11 shows a photoelectron spectrum obtained at the main ion-current peak (at 374·7 nm), indicating a photoelectron energy distribution that largely deviates from the normal Franck–Condon pattern of the $\Delta v=0$ ionization transition. The $v^+=0,1,2$ photoelectron bands in figure 11 are due to three-photon absorption, whereas the $v^+=4$ band results from four-photon absorption. This photoelectron spectrum suggests that autoionization takes place at the three-photon energy level and four-photon absorption is enhanced at this autoionizing level (Achiba and Kimura 1984 b). Its possible electronic state is considered as A' $^2\Sigma^+$ $(2\sigma^2 3\pi^4 3\sigma)$, allowed by one photon from the Rydberg A $^2\Sigma^+$ state (Achiba and Kimura 1984 b).

In general, $(n+1)$ resonant ionization should be most important for the study of autoionization, since there is no chance of accidental double resonance below the ionization threshold. Anomalous photoelectron intensity distributions are also observed for the N_2 molecules in (3+1) resonant ionization via the resonant b $^1\Pi_u$ state (Pratt *et al.* 1984 b). In this case, the anomalous photoelectron patterns have been discussed in terms of complex interactions among the intermediate levels.

5.2. *Autoionization of NO via non-Rydberg B v'=9 state*

As far as one-electron transitions are concerned, the ionization transition producing the NO^+ ground state from the non-Rydberg B $^2\Pi$ is electronically forbidden, since it requires a two-electron transition. The electron configuration of the B $^2\Pi$ state is $5\sigma^2 1\pi^3 2\pi^2$, while the ground state (X $^2\Pi$) of NO^+ is $5\sigma^2 1\pi^4$. The lowest allowed ionic state produced by one-electron ionization from the B $^2\Pi$ state is the a $^3\Sigma^+$ state, 6·5 eV above the ground state of NO^+. Therefore, the region below the a $^3\Sigma^+$ state of NO^+ is the forbidden area (shaded in figure 9 (*f*)) in this sense.

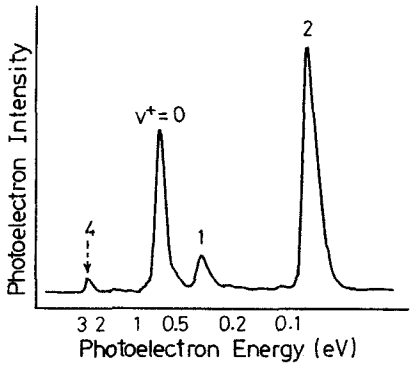

Figure 11. Photoelectron spectrum of autoionization for NO (Achiba *et al.* 1985), obtained by (2+1) resonant ionization via the Rydberg A $^2\Sigma^+$ $v'=4$ state. This corresponds to the process (*b*) in figure 9.

The $v'=9$ level of the B $^2\Pi$ state has been chosen as a resonant intermediate state to study autoionization (Achiba *et al.* 1985), since this level does not interact with any Rydberg states. If an MPI ion-current signal is produced by one-photon absorption from the B $^2\Pi$ $v'=9$ state, it seems to be responsible for autoionization. In fact, a weak MPI ion-current spectrum can be observed in the region 369·0–370·5 nm, as shown in figure 12, indicating a number of peaks attributable to the rotational progressions of the resonant B $v'=9$ state. The rotational lines are explained partly in terms of a normal Boltzmann distribution at a temperature of about 220 K. However, as seen from figure 12, anomalous intensity enhancement occurs at several rotational bands shaded in the spectrum.

Two types of photoelectron spectra have been observed at the rotational peaks of the B $^2\Pi$ $v'=9$ ion-current spectrum (Achiba *et al.* 1985), as shown in figure 13. The photoelectron spectra (*a*) and (*b*) in figure 13 are obtained at the normal and the anomalous ion-current peaks, respectively. The vibrational distribution of these photoelectron spectra show non-Franck–Condon behaviour, suggesting that autoionization occurs in both cases. The $v^+=0, 1, 2$ photoelectron bands mainly result from autoionizations which occur at the three-photon energy levels, whereas a weak $v^+=6$ photoelectron band is produced by four-photon absorption. The appearance of the $v^+=6$ band indicates that four-photon absorption is enhanced at the three-photon autoionizing discrete level. With increasing laser power, the $v^+=6$ band intensity increases with respect to the other vibrational bands (Achiba *et al.* 1985).

The photoelectron spectra in figure 13 are attributed to autoionization which take place at neutral valence-excited states allowed by one-electron transition from the B $^2\Pi$ state. The possible valence states responsible for the autoionizations are the B′ $^2\Pi$ and I $^2\Sigma^+$ states with the same electronic configuration (Achiba *et al.* 1985). Electronic transition between the B $^2\Pi$ and B′ $^2\Pi$ states has been observed earlier in an emission study (Huber 1964). According to theoretical and experimental studies (Bardsley 1983, Miescher 1976), both B′ $^2\Delta$ and I $^2\Sigma^+$ states have 'repulsive potential curves' crossing the $NO^+(X\,^2\Sigma^+)$ potential curve near its minimum, as schematically shown in figure 10.

If the three-photon energy matches with a rotational level of a specific discrete autoionizing state within several cm^{-1}, the corresponding MPI ion-current line should be enhanced. Therefore, an anomalous-intensity ion-current line is expected to appear

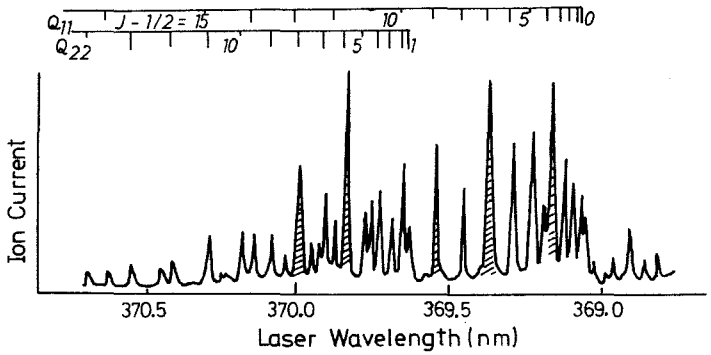

Figure 12. Rotationally resolved MPI ion-current spectrum of the NO molecule (Achiba *et al.* 1985), obtained by (2 + 1) resonant excitation via the valence-excited B $^2\Pi$ $v'=9$ state. This corresponds to the process (*f*) shown in figure 9. Anomalous-intensity peaks (shaded) are observed, together with normal-intensity peaks. Both types of rotational peak are due to autoionization.

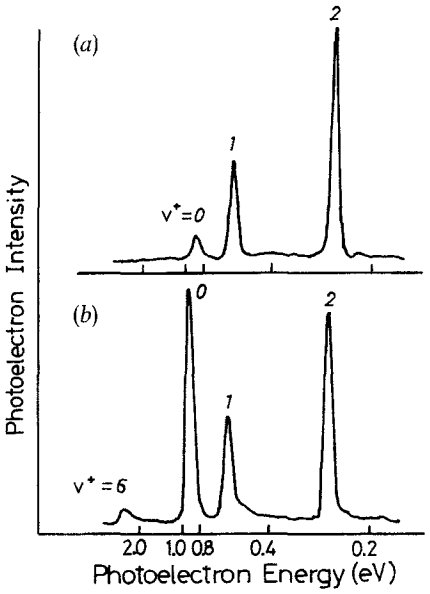

Figure 13. Photoelectron spectra of NO (Achiba *et al.* 1985), observed at the two kinds of the MPI peak shown in figure 12: (*a*) at one of the normal-intensity peaks, and (*b*) at one of the anomalous-intensity peaks.

at each accidental double resonance, overlapping with one of the normal rotational peaks, as seen from figure 12. The most probable candidate for the double-resonant state embedded in the ionization continuum is the $v'=6$ level of the Rydberg N ($^2\Delta$) state, which is allowed by one photon from the B $^2\Pi$ state. The N $^2\Delta$ $v'=6$ state is located at the three-photon level, as seen from figure 10.

The observed autoionization for the B $^2\Pi$ $v'=9$ state can be explained in terms of electronic autoionization which involves electronic coupling between a dissociative portion of the valance excited state and the ionization continuum (Achiba *et al.* 1985). Generally speaking, in electronic autoionization, photoelectron vibrational distribution is governed by a Franck–Condon overlap of the vibrational wavefunctions between the autoionizing and the ionic state (Berkowitz 1979, Eland 1980). The important role of valence-excited states in the autoionization process of NO near the ionization threshold has been pointed out (Jungen 1966, Guisti-Suzor and Jungen 1984).

On the basis of the autoionization mechanism of Guisti-Suzor and Jungen (1984), the autoionization from the discrete Rydberg N $^2\Delta$ $v'=6$ state has been explained in terms of 'indirect electronic coupling' between this discrete state and the ionization continuum through a dissociative part of the valence-excited B′ $^2\Delta$ state (Achiba *et al.* 1985). In other words, the Rydberg N $^2\Delta$ $v'=6$ state initially couples electronically with the dissociative part of the B′ $^2\Delta$ state with the same symmetry, and then the dissociative B′ $^2\Delta$ state couples electronically with the ground-state ion. The observed large deviation of the photoelectron spectra from the $\Delta v=1$ propensity rule, which is widely accepted for vibrational autoionization, seems to be strong experimental evidence for the indirect autoionization mechanism.

The MPI ion-current intensities in the B $^2\Pi$ $v'=9$ region are almost three orders of magnitude lower than that in the Rydberg C $^2\Pi$ $v'=1$ region (Achiba *et al.* 1985). This fact suggests that autoionization from the dissociative state (I or B′) is considered to proceed in competition with a very fast neutral dissociation process such as $NO^* \rightarrow N + O$.

5.3. *Autoionization of NO via Rydberg C state*

When NO is excited by a single laser (two photons) to the $v'=4$ level of the Rydberg C $^2\Pi$ state, then the molecule is ionized by the third photon producing the $v^+=4$ of $NO^+(X)$. However, when NO is excited to the same resonant level (C $^2\Pi$ $v'=4$) by one laser and then further excited by another laser in the region 560–580 nm, the total photon energy does not exceed the $v^+=4$ level of NO^+. This corresponds to process (*c*) shown in figure 9. Such two-colour experiments have been carried out (Achiba and Kimura 1984 b), and the MPI ion-current spectrum shown in figure 14 has been obtained. The three kinds of sharp bands in figure 14 are attributed to the autoionizing states 6s σ ($v'=4$), 5d δ ($v'=4$), and 5d σ, π ($v'=4$) states. These super-excited states have been found earlier from a VUV absorption study (Miescher and Alberti 1976). Figure 15 shows photoelectron spectra observed at the three MPI ion-current peaks shown in figure 14, indicating again anomalous photoelectron patterns which are associated with the autoionization. The $v^+=4$ photoelectron peak is observed in each case, again indicating that fourth-photon absorption is enhanced at the three-photon autoionizing state.

6. Intramolecular relaxation

A large number of experimental and theoretical studies have been carried out on radiationless decay processes and unimolecular relaxation mechanisms for vibrationally excited molecular electronic states (for example, Parmenter 1982). Intramolecular relaxation processes such as vibrational redistribution (IVR), internal conversion, intersystem crossing in molecular excited electronic states have been studied widely by optical emission spectroscopy. In resonant multiphoton ionization of molecules under collision-free conditions, the ionization transition of a resonant intermediate state in principle takes place in competition with radiative or nonradiative intramolecular relaxation, as mentioned before in Section 2.

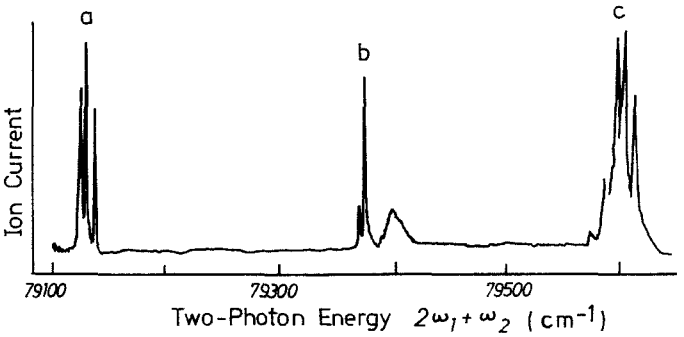

Figure 14. Two-colour MPI ion-current spectrum of NO (Achiba and Kimura 1984 b), obtained by resonant ionization via the Rydberg C $^2\Pi$ $v'=4$ state. This corresponds to the process (*e*) in figure 9. The MPI peaks correspond to the autoionizing levels: (*a*) 6sσ $v'=4$, (*b*) 5dδ $v'=4$, and (*c*) 5dσ, π $v'=4$.

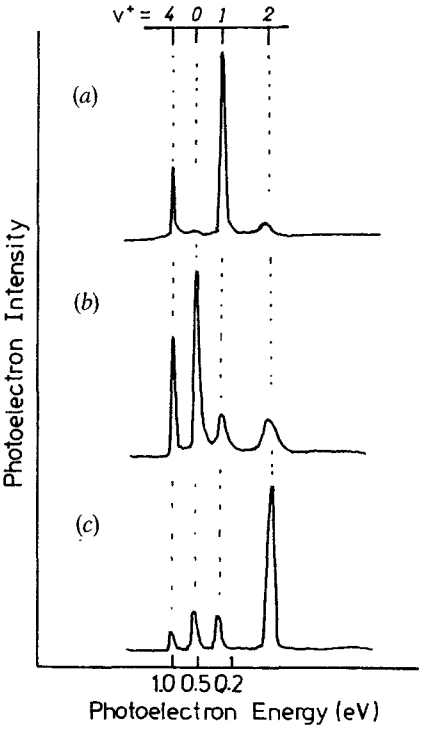

Figure 15. Photoelectron spectra of the autoionization of NO (Achiba and Kimura 1984 b), observed at the MPI peaks (*a*)–(*c*) shown in figure 14.

The author and coworkers (Achiba *et al.* 1983 b, 1984 a, Hiraya *et al.* 1985) have employed an excited-state photoelectron spectroscopic technique to deduce information about relaxation phenomena of highly vibrationally excited molecular electronic states of benzene and naphthalene under collision-free conditions. The technique has been found to be useful in studies of relaxation phenomena of excited states.

In this Section, photoelectron spectroscopic results demonstrating evidence for intramolecular vibrational redistribution and internal conversion, are described in the following four cases; (1) IVR of the S_3 state of benzene, (2) IVR of the S_1 states of benzene, (3) IVR of the S_1 state of naphthalene, and (4) internal conversion of the S_2 state of naphthalene.

6.1. *IVR in the S_3 state of benzene*

Photoelectron spectra of excited benzene molecules under collision-free conditions have been observed with a nanosecond laser in the wavelength region 471–513 nm (Achiba *et al.* 1983 b). In this region, four photons are required for ionizing benzene. The molecule is initially excited by two photons to several low-lying vibronic levels of the S_1 ($^1B_{2u}$) state, at which IVR is not significant compared to up-pumping. The molecule is then further excited by the third photon to the S_3 ($^1E_{1u}$) state at vibrationally excited levels, and finally it is ionized by the fourth photon to eject photoelectrons. The overall ionization process is schematically shown in figure 16.

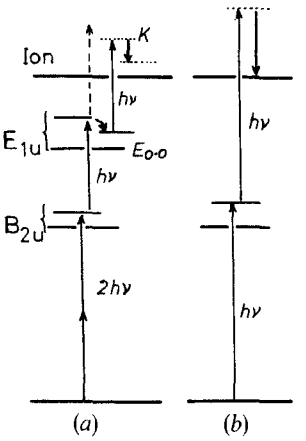

Figure 16. Schematic energy level diagram of benzene, showing (*a*) four-photon resonant ionization and (*b*) two-photon resonant ionization.

A series of photoelectron spectra thus obtained by four photons under such experimental conditions has indicated that single prominent photoelectron bands are observed and their kinetic energies are given by the linear relationship $K_{exp}=h\nu-C$, where $h\nu$ is the one-photon energy and C is a constant independent of the laser wavelength. In other words, the observed photoelectron energy depends only on the one-photon energy, in spite of the four-photon ionization. From this relationship, it has been concluded that ionization takes place after rapid relaxation at the three-photon intermediate state (Achiba *et al.* 1983 b). As seen from figure 16(*a*), the overall ionization process can be expressed by (2+1+1). The observed prominent photoelectron bands are attributable to $\Delta v=0$ ionization transitions which occur from the three-photon relaxed states.

The photoelectron kinetic energy in this case is calculated by the formula

$$K=h\nu+E_{0\text{-}0}-I_a+\varepsilon_1-\varepsilon_2 \tag{7}$$

where I_a is the adiabatic ionization energy of benzene, $E_{0\text{-}0}$ is the 0-0 energy of the electronically excited state associated with the three-photon levels, and ε_2 and ε_2 are the internal energies of the relaxed state and the final ionic state, respectively. The prominent photoelectron bands are considered to be due to $\Delta v=0$ ionization transitions, as mentioned before, so that ε_1 is approximately equal to ε_2. In other words, the internal energy can be assumed to be unchanged upon ionization in this case. Therefore, from equation (7), the photoelectron energy is simply given by

$$K=h\nu+E_{0\text{-}0}-I_a \tag{8}$$

From the observed photoelectron energies and the ionization potential of benzene, an average value of $E_{0\text{-}0}=6{\cdot}97$ eV has been deduced from equation (8) (Achiba *et al.* 1983 b). This value is in reasonable agreement with the $E_{0\text{-}0}$ energy of the $^1E_{1u}$ state (6·87 eV) estimated earlier from an absorption study (Wilkinson 1956). The above-mentioned example indicates that the 0-0 energy of an excited electronic state can be determined by photoelectron spectroscopy.

The overall symmetry of the $\nu_{14}(b_{2u})$ and $\nu_{18}(e_{1u})$ levels of the $^1B_{2u}$ state are $b_{2u}\times B_{2u}=A_{1g}$ and $e_{1u}\times E_{2u}=E_{2g}$, so that one-photon absorption from the $^1B_{2u}$

vibronic levels to the $^1E_{1u}$ state is allowed. This symmetry consideration supports the above assignment of the three-photon states to the $^1E_{1u}$ vibronic states. Therefore, on the basis of the photoelectron study, it has been concluded that IVR takes place within the $^1E_{1u}$ state and much faster than the up-pumping process indicated by a broken arrow in figure 16 (Achiba *et al.* 1983 b). The up-pumping rate is estimated to be 10^{10}–$10^{11}\,s^{-1}$ at a laser intensity of 10^8–$10^9\,W/cm^2$, by assuming an ionization cross-section of the order of $10^{-17}\,cm^2$. The intramolecular decay rate of the $^1E_{1u}$ state of benzene in a matrix at 4 K has been evaluated to be $10^{14}\,s^{-1}$ from absorption spectra (Katz *et al.* 1970). This decay rate is therefore three to four orders of magnitude greater than the above-mentioned up-pumping rate estimated under collision-free conditions.

The photoelectron bands observed in the ionization process shown in figure 16 are broad compared with those of $\Delta v=0$ ionization observed for optically prepared single vibrational levels. Considering that the internal energy remains unchanged upon the $\Delta v=0$ ionization transition, the observed broadening of the prominent photoelectron bands can be explained in terms of overlapping of various $\Delta v=0$ ionization transitions of the vibrationally relaxed $^1E_{1u}$ states. From such a photoelectron spectroscopic study, it has been concluded that fast intramolecular vibrational relaxation takes place within the three-photon $^1E_{1u}$ excited states (Achiba *et al.* 1983 b).

The abovementioned $^1B_{2u}$ $14_0^1 1_0^n$ vibrational levels below the $n=3$ level are fairly low in vibrational energies, so that IVR at these levels is insignificant compared with up-pumping. A photoelectron spectroscopic study for higher $14_0^1 1_0^n$ vibrational levels, at which IVR is known to occur significantly, is described in the following Section.

6.2. *Benzene S_1 state*

One of the most puzzling problems in the field of radiationless transitions is a sharp decrease in the fluorescence quantum yield of the S_1 state of benzene above $\Delta E=3000\,cm^{-1}$. This phenomenon has been called 'channel three' in the literature (for example, Parmenter and Schuyler 1970, Selinger and Ware 1970, Callomon *et al.* 1972, Yoshihara *et al.* 1984). Most of the arguments concerning the nonradiative pathway in benzene responsible for channel three have been based on fluorescence emission and absorption line broadening (for example, Parmenter 1972). Spectral broadening with increasing internal excess energy has been observed in dispersed fluorescence spectra for many large molecules under collision-free conditions, and explained in terms of IVR processes which change the nature of the emitting states (for example, Smalley 1983). Similar band broadening has also been observed in MPI ion-current spectra for the S_1 vibronic levels of benzene in supersonic jets (Muraki *et al.* 1980, Aron *et al.* 1980).

Photoelectron spectra for a series of benzene S_1 vibronic levels ($6^1 1^n$, $n=2$–5) whose internal excess energies are up to $\Delta E=5000\,cm^{-1}$ have been obtained by a (1+1) resonant ionization technique under collision-free conditions (Achiba *et al.* 1984 a). The photoelectron spectra thus obtained are shown in figure 17, indicating spectral broadening with increasing internal excess energy. Such broadening of the photoelectron bands has been explained in terms of IVR within the S_1 state above the onset of channel three (Achiba *et al.* 1984 a).

The relative band intensities of the MPI ion-current spectrum for the $6^1 1^n$ ($n=2$–5) vibronic levels are very similar to those of the absorption spectrum, but considerably different from that of the fluorescence excitation spectrum. The ionization yields are almost unity over the vibronic bands up to $\Delta E=5000\,cm^{-1}$ (Achiba *et al.* 1984 a).

Excited-state photoelectron spectra have been reported for some low-lying vibrational S_1 levels (below $\Delta E=1500\,cm^{-1}$), at which essentially no band broadening

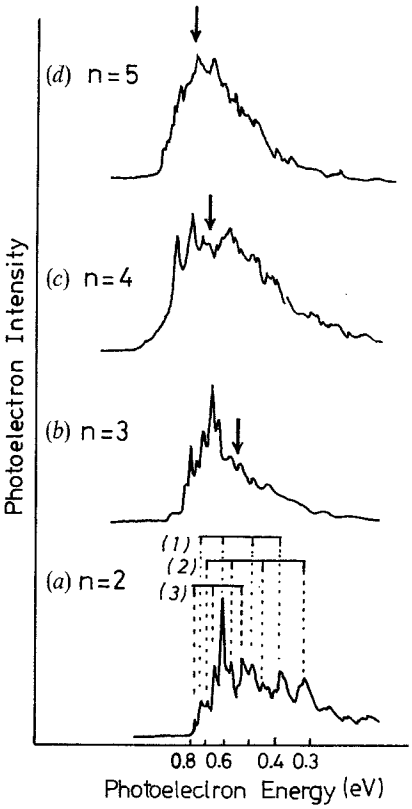

Figure 17. Photoelectron spectra of benzene (Achiba *et al.* 1984 a), obtained by resonant ionization via the vibronic levels $6^1 1^n$ ($n=2$–5) of the S_1 state. The vibrational energies (ΔE) are; (*a*) 2367 cm^{-1} at $n=2$, (*b*) 3290 cm^{-1} at $n=3$, (*c*) 4213 cm^{-1} at $n=4$, and (*d*) 5136 cm^{-1} at $n=5$. An arrow indicates the position of $\Delta v=0$ ionization. In spectrum (*a*), the numbers in parentheses 1–3 indicate the progressions of $6_1^1(3/2)1_2^n$, $6_1^1(1/2)1_2^n$, and $6_1^0 1_2^n$, respectively.

is observed (Long *et al.* 1983). The resulting photoelectron bands have been interpreted in terms of the ν_1 and ν_6 vibrations of the benzene cation. As seen from figure 17 (*a*), the photoelectron spectrum obtained at the $n=2$ level of the $6^1 1^n$ series ($\Delta E=2367\ cm^{-1}$) indicates many peaks which can be attributed to the $6_1^1 1_2^n$ and $6_1^0 1_2^n$ progressions of the benzene cation. Therefore, the photoelectron spectrum (*a*) in figure 17 reflects mostly the optically prepared resonant states.

However, the photoelectron spectra observed at the $n=3$–5 levels of the S_1 $6^1 1^n$ series (figure 17) show more or less broad structureless bands, broadening with increasing excitation energy. Several sharp photoelectron peaks appearing at the lower vibronic level (for example, $n=2$) are not observed at $n=5$. If very fast IVR occurs at a resonant intermediate state, its photoelectron spectrum would lose the memory of the optically prepared state, and it reflects vibrationally relaxed states. As mentioned in Section 2, ionization transition from any vibrationally relaxed state is allowed, and governed by Franck–Condon overlap between the resonant state and the ionic state. The $\Delta v=0$ ionization is the most probable transition, when the geometrical change upon ionization is small.

The IVR process populates many kinds of vibrational modes and quantum states, which are isoenergetic with the optically prepared state. Therefore, superposition of many $\Delta v = 0$ ionization transitions should broaden the photoelectron bands, giving rise to the band maxima at $\Delta v = 0$. The positions of the expected $\Delta v = 0$ ionization transitions are indicated by arrows in figure 17. The photoelectron spectrum (*c*) obtained at $n = 4$ in figure 17 shows two sharp peaks, which can be attributed to the $6_1^1 1_4^3$ and $6_1^1 1_4^2$ vibrations of the benzene cation. The intensity ratio of the sharp peak to the broad band in each photoelectron spectrum roughly provides a measure of the ratio of the ionization rate (k_i) to the IVR rate (k_{IVR}). The rate of ionization for the S_1 state of benzene is thereby estimated to be the order of magnitude of 10^{10}–$10^{11}\ s^{-1}$ under the laser conditions used (Achiba *et al.* 1985). Therefore, the IVR rate at the $S_1\ 6^1 1^4$ level ($\Delta E = 4213\ cm^{-1}$) is considered to be about the same order of magnitude (10^{10}–$10^{11}\ s^{-1}$).

The lifetimes of the single vibronic levels above the channel-three region have been discussed on the basis of absorption line widths (Callomon *et al.* 1972). According to the line-width measurements, the decay rate of the $6^1 1^4$ level of the S_1 state of benzene has been estimated to be $2{\cdot}45 \times 10^{11}\ s^{-1}$, which is in agreement with the abovementioned photoelectron spectroscopic value (10^{10}–$10^{11}\ s^{-1}$). The k_{IVR} value is considered to be equal to or less than $2{\cdot}45 \times 10^{11}\ s^{-1}$ at the $6^1 1^4$ level. Therefore such photoelectron spectroscopic estimation for k_{IVR} seems to be helpful for studying intramolecular decay processes of nonradiative excited states. As the laser power decreases, the intensity of the sharp feature in figure 17 decreases, whereas the intensity of the broad band increases (Achiba *et al.* 1984 a). This intensity change can be understood by recalling that the ionization rate is changeable with the laser power.

The rate of IVR (k_{IVR}) increases significantly with the increasing vibrational energy of the S_1 state, and at the $n = 5$ vibronic level ($\Delta E = 5000\ cm^{-1}$) it must be considerably larger than the rate of ionization ($k_i = 10^{10}$–$10^{11}\ s^{-1}$). The rate of internal conversion (k_{ic}') is considered to be of lower order than $10^{11}\ s^{-1}$. The photoelectron study also indicates that the vibrationally redistributed S_1 state has a certain lifetime longer than 10^{11} s, even at $\Delta E = 5000\ cm^{-1}$ (Achiba *et al.* 1984 a).

6.3. *Intramolecular relaxation of S_1 of naphthalene*

Resonant ionization of naphthalene via several single vibronic levels of the S_1 state (up to the internal energy $\Delta E = 2500\ cm^{-1}$) has been studied by photoelectron spectroscopy (Hiraya *et al.* 1985). This photoelectron study indicates that IVR occurs at vibronic levels higher than $\Delta E = 2200\ cm^{-1}$. Figure 18 shows two-colour photoelectron spectra obtained for (1 + 1) resonant ionization of naphthalene via the $\bar{7}^1$ and $\bar{8}^1 8^1$ levels of the S_1 state. These two-colour spectra in figure 18 were deduced by subtracting the one-colour photoelectron feature observed by the first laser alone from the photoelectron spectra obtained by two lasers. Spectrum (*a*) in figure 18 is obtained by tuning the first laser (ω_1) to 303·8 nm (the $\bar{7}^1$ level) and the second laser to 288·1 nm; no significant signal appears with the second laser alone.

The one-colour photoelectron spectra obtained for a series of higher vibronic levels are shown in figure 19. Spectrum (*a*) in figure 19 clearly shows three single photoelectron bands including the $\Delta v = 0$ ionization band whose bandwidth is $65\ cm^{-1}$. The photoelectron bands observed at the fairly low-lying vibronic levels ($\Delta E < 200\ cm^{-1}$) can be interpreted in terms of several cation vibrational levels which are produced by $\Delta v = 0, \pm 1, \ldots$ ionization transitions of the optically prepared vibronic levels.

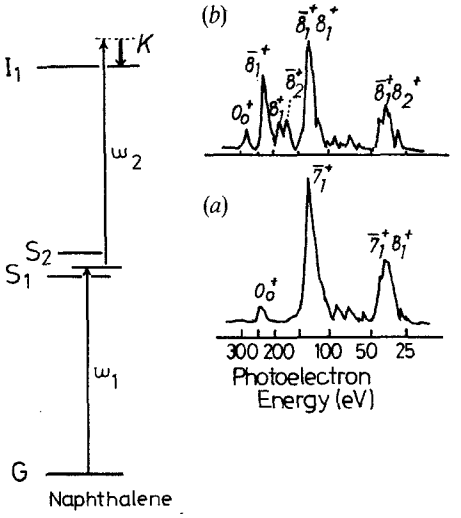

Figure 18. Schematic energy level diagram of naphthalene, relevant to two-colour, two-photon resonant ionization, and photoelectron spectra observed at two vibronic levels of the S_1 state (Hiraya *et al.* 1985): (*a*) $\bar{7}^1$ (910 cm^{-1}) and (*b*) $\bar{8}^1 8^1$ (1135 cm^{-1}).

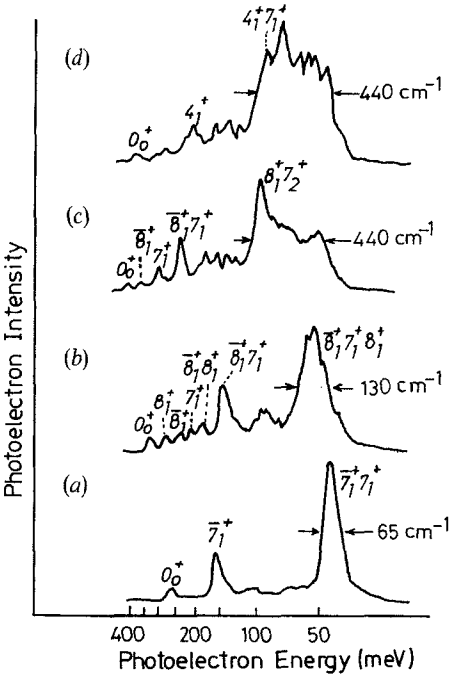

Figure 19. Photoelectron spectra of naphthalene (Hiraya *et al.* 1985), obtained by (1+1) resonant ionization via higher vibronic S_1 levels: (*a*) $\bar{7}^1 7^1$ ($\Delta E = 1894$ cm^{-1}), (*b*) $\bar{8}^1 7^1 8^1$ (2122 cm^{-1}), (*c*) $\bar{8}^1 7^2$ (2410 cm^{-1}), (*d*) $4^1 7^1$ (2421 cm^{-1}).

However, the broad photoelectron bands appearing at the higher vibronic levels ($\Delta E > 2000\,cm^{-1}$) cannot be explained simply in terms of ionization of the optically prepared vibronic levels. With increasing internal energy, the photoelectron band becomes broader, as seen from figure 19. Such band broadening has been explained in terms of IVR within the S_1 manifold (Hiraya *et al.* 1985). The isoenergetic levels redistributed by IVR should be dominated by overtones and/or combinations of many low-frequency vibrational modes. Therefore, the $\Delta v = 0$ ionization transitions are the most probable for the redistributed levels. Overlap of many $\Delta v = 0$ ionization transitions gives rise to band broadening in the photoelectron spectrum.

In general, IVR takes place in competition with other relaxation processes at the optically prepared vibronic level. The fluorescence lifetime of naphthalene at higher vibronic levels of the S_1 state is 10^{-7} s. In the photoelectron spectra, the rate of ionization depends on the laser power. If the rate of IVR is much slower than the rate of ionization at a single vibronic level, then the resulting photoelectron spectrum should reflect the single vibronic level rather than vibrationally relaxed states.

As seen from figures 19 (*b*)–(*d*), many narrow photoelectron bands appear; these can be assigned to the ionizations of optically prepared, single vibronic levels. The appearance of both the sharp and the broad features in figure 19 indicates that IVR takes place in competition with the up-pumping under the laser conditions used.

6.4. *Internal conversion at the S_2 origin*

The photoelectron spectrum of naphthalene obtained by one-colour (1+1) resonant ionization via the S_2 origin is shown in figure 20, indicating an extremely broad feature (Hiraya *et al.* 1985). If ionization of the optically prepared S_2 origin is much faster than other relaxation processes, the resulting spectrum reflects the vibrational character of the S_2 origin. In this case, the photoelectron spectrum would show a peak due to the 0_0^+ ion because of its favourable Franck–Condon overlap expected from the vibrationless S_2 state.

However, as seen from figure 20, no photoelectrons due to the 0_0^+ ion have been detected (Hiraya *et al.* 1985). Instead, the photoelectron spectrum in figure 20 shows a peak which can be expected from rapid internal conversion. In other words, the ionization takes place from the vibrationally excited S_1 state isoenergetic with the S_2 origin, and no ionization occurs from the S_2 vibrationless state. From these results, the

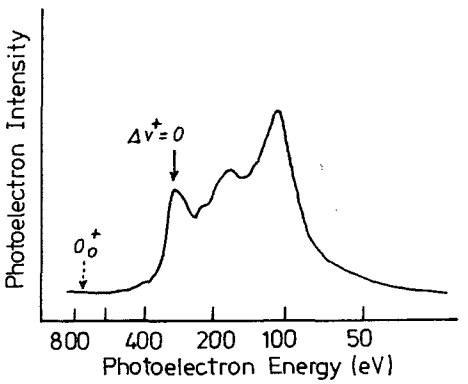

Figure 20. Photoelectron spectrum of naphthalene (Hiraya *et al.* 1985), obtained by (1+1) resonant ionization via the S_2 origin region ($3982\,cm^{-1}$ above the S_1 origin).

following conclusions have been deduced (Hiraya *et al.* 1985). (1) Electronic relaxation is faster than ionization at the optically prepared S_2 level. (2) Ionization occurs from many vibrationally excited S_1 levels produced by internal conversion. The rate of ionization (k_i) under the laser conditions used is estimated to be about $10^{11}\,s^{-1}$. Therefore, the rate of internal conversion should be greater than $10^{11}\,s^{-1}$.

7. Other applications

Photoionization selectivity plays an important role in generating state-selected ions. In general, a vibrationally and rotationally resolved ionic state can be produced by selecting an appropriate excited state as resonant intermediate excited state in resonant multiphoton ionization of molecules.

For example, when a Xe atom is ionized by (3 + 1) resonant ionization through the $5d[2\,1/2]^0_3$ Rydberg state, a photoelectron study indicates that only the $^2P_{3/2}$ state of Xe^+ is produced (Sato *et al.* 1984 a). This is in contrast to one-photon VUV photoelectron spectroscopy, in which both the $^2P_{3/2}$ and $^2P_{1/2}$ states of Xe^+ are always produced. This indicates that removal of the Rydberg electron does not induce the relaxation of core electrons.

Photoelectron vibrational structure in the ionization of an excited molecule is governed by Franck–Condon factors between the excited state and the ionic state. When a Rydberg state not perturbed by other excited states is selected as a resonant intermediate state, the $\Delta v=0$ ionization transition takes place dominantly, since removal of the Rydberg electron essentially does not change the molecular geometry. Such a situation has been demonstrated clearly for ammonia (Achiba *et al.* 1981 b, 1983 a, Glownia *et al.* 1982, Conaway *et al.* 1985): the $NH_3{}^+(X)$ ions at $v^+=0, 1, 2\ldots$ are dominantly produced by ionization, for example, from the Rydberg C′ state at $v'=0, 1, 2\ldots$, respectively. Similar situations also occur for some diatomic molecules in $(n+1)$ resonant ionizations via the Rydberg C $^2\Pi$ $v'=0, 1$ levels of NO (Miller and Compton 1981 a); the Rydberg F $^2\Delta$ $v'=0, 1$ and H $^2\Sigma^+$ $v'=0, 1$ levels of NO (Achiba *et al.* 1983 a); the Rydberg C $^1\Pi_u$ $v'=0$–4, $J'=1$ levels of H_2 (Pratt *et al.* 1984 a); and Rydberg o_3 $^1\Pi_u$ $v'=1, 2$ levels of N_2 (Pratt *et al.* 1984 b). However, some systematic departures from expected Franck–Condon factors have been observed even for $(n+1)$ resonant ionization via some Rydberg states, for example, in the case of the Rydberg C $^1\Pi_u$ $v'=0$–4, $J'=1$ state of H_2.

Vibrationally resolved photoelectron spectra of polyatomic molecules resulting from (1 + 1) resonant ionization via the S_1 states provide detailed information about vibrational models of parent ions, as indicated for benzene (Long *et al.* 1983), aniline (Meek *et al.* 1986), chlorobenzene (Anderson *et al.* 1982), and naphthalene (Hiraya *et al.* 1985). It should be mentioned that in general when a specific vibronic mode is selected, information about the same vibronic mode and related modes of the parent ion can be deduced from photoelectron spectra.

Deviation from expected Franck–Condon factors in $(n+1)$ resonant ionization is attributed to autoionization or configuration mixing of the resonant state. In $(n+2)$-type resonant ionization, there would be a possibility of accidental resonance, and hence the situation would be complicated. Such resonant ionization should be avoided in photoelectron studies. In fact, a complicated situation has been demonstrated for (3 + 2) and (3 + 3) resonant ionization of CO via the Rydberg A $^1\Pi$ $v'=1$–3 state (Pratt *et al.* 1983 a).

Some complication of photoelectron vibrational structure for (2 + 2) resonant ionization of NO via the Rydberg A $^2\Sigma^+$ $v'=0, 1$ state has been reported (Kimman *et al.*

1982, White *et al.* 1984). In this (2+2) case, the photoelectron vibrational structure suggests that strong accidental resonance occurs at the third photon state (White *et al.* 1984). Formation of $NO^+(X)$ at $v^+=0$ and $v^+\geqslant 3$ in (3+2) resonant ionization of NO via the Rydberg C $^2\Pi$ $v'=0$ state has been ascribed to significant perturbations by the nearly degenerate valence-excited B $^2\Pi$ $v'=7$ level (White *et al.* 1982).

Three mechanisms are known for ionic fragmentation in resonant ionization: (1) ionization of neutral fragments, (2) fragmentation of parent ions, and (3) dissociative ionization via an autoionizing state. In connection with these mechanisms, photoelectron spectra observed for (3+1) resonant ionization of H_2S via Rydberg states indicate that HS^+ and S^+ ions are produced mainly by additional photon absorption from the ground-state H_2S^+ ion at the $v^+=0$ and 1 levels, respectively (Achiba *et al.* 1982).

In multiphoton ionization of CCl_2F_2 and CCl_3F by an ArF laser, formation of the CF radical has been suggested from photoelectron energy analysis (Hepburn *et al.* 1982). In (1+1) resonant ionization of benzene and benzaldehyde, identical photoelectron spectra have been observed, suggesting that the benzene cation is generated from benzaldehyde (Long *et al.* 1983). Mechanisms of ionic photofragmentation for molecules in photochemistry are interesting subjects to be studied by this technique. Unimolecular dissociation rates of the chlorobenzene cation prepared by multiphoton ionization have been studied in the region 265–270 nm (Durant *et al.* 1984). Decomposition in this region proceeds by two-photon ionization followed by one-photon absorption.

Photoelectron kinetic energy measurements for resonant multiphoton ionization are also useful for determining the vibrationless level of a resonant excited state. In principle, this can be determined by extrapolating photoelectron energies plotted as a function of laser photon energy for a series of the resonant vibronic levels. Determination of vibrationless levels by this method has been tested for the E_{1u} state of benzene (Achiba *et al.* 1983 b) and the S_2 state of triethylamine (Kawasaki *et al.* 1985).

Photodissociation of the NO dimer producing the Rydberg A $^2\Sigma^+$ state of NO has been studied by measuring photoelectron spectra of (1+1) resonant ionization of this state via the higher Rydberg F $^2\Delta$ state (Sato *et al.* 1986). Several Van der Waals complexes produced in supersonic jets have been studied by photoelectron spectra of (1+1) and (2+1) resonant ionization. The adiabatic ionization potential of ArNO and the dissociation energy of $ArNO^+$ have been determined from photoelectron spectra by (1+1) resonant ionization through the Rydberg C state (Sato *et al* 1984 b). A photoelectron study of several hydrogen-bonded complexes of phenol and 7-azaindole with water molecules by (1+1) resonant ionization via the S_1 state origin indicates considerable differences between the threshold and the vertical ionization potentials, probably because of significant geometric change upon ionization (Fuke *et al.* 1984). The lower limits of dissociation energies for $ArXe^+$ and $KrXe^+$ have been determined from photoelectron spectra of (2+1) resonant ionization of ArXe and KrXe in jets (Pratt *et al.* 1985 b, c). In the case of KrXe, the photoelectron spectra show a number of peaks due to predissociation of the resonant intermediate state followed by photoionization of the excited atomic fragment in addition to photoelectron peaks due to $KrXe^+$.

Photoelectron angular distribution of resonant multiphoton ionization should provide important information on characterization of resonant intermediate states of molecules. A considerable number of papers have been published on rare-gas atoms and alkali atoms. Concerning photoelectron angular distribution of molecular excited states, only a few studies have been reported: the Rydberg F $^2\Delta$ $v'=1$ level of NO and

the Rydberg C' $^1A_1$ level of NH_3 (Achiba *et al.* 1983 a); the valence-excited B $^2\Pi$ $v'=9$, Q_{11}, $J=3\frac{1}{2}$ and Q_{22}, $J=6\frac{1}{2}$ levels of NO (Achiba *et al.* 1985); the E, F $v'=0, 1, 2$, $J=0, 1$ levels of H_2 (Anderson *et al.* 1982). Photoelectron angular distribution has also been reported for (2+2) resonant ionization of NO via the A $^2\Sigma^+$ $v'=0, 1$ levels (White *et al.* 1984). In such (2+2)-type resonant ionization, the photoelectron work in general provides information about the third-photon state rather than the second-photon state.

8. Concluding remarks

In studies of resonant multiphoton ionization ($M \rightarrow M^* \rightarrow M^+ + e^-$), ion-current and mass-spectroscopic information has been widely obtained from U.V./visible laser experiments, but there are still only a limited number of photoelectron studies. As described in the present article, photoelectron measurements provide unique information about resonant excited states and ionic states, important for their characterization or diagnosis. In addition to photoelectron kinetic-energy distribution, one can also obtain photoelectron branching ratios for producing different ionic states, as well as photoelectron angular distribution. This information will be valuable for studying the dynamic behaviour of molecular excited states.

The excited-state photoelectron studies so far published suggest the versatility of this technique and indicate the potential of its future application to explore processes of photophysics and photochemistry associated especially with molecular nonradiative excited electronic states. Combination of the supersonic-jet technique with laser photoelectron spectroscopy provides possibilities for studying various types of molecular complexes.

Information on well-defined ionic states available from conventional VUV photoelectron spectroscopy is helpful for dynamic photoelectron spectroscopy. However, selecting a specific resonant excited state, one can produce a specific ionic state on the basis of ionization selection rules. As mentioned before, $(n+1)$-type resonant ionization is especially important in dynamic photoelectron spectroscopy, in order to avoid accidental resonance at the final ionization stage. Such a resonance condition can often be created by a single laser. However, the use of two lasers, the so-called two-colour experiment, is most desirable for this purpose, although it requires a more sophisticated technique. It is important to ionize a molecule by a single photon from a resonant excited state in dynamic photoelectron spectroscopy.

A nanosecond laser has so far been employed as excitation/ionization source but use of a picosecond laser will make it possible to study faster phenomena. Picosecond photoelectron spectroscopy would provide new information about the dynamic behaviour of highly excited electronic states which cannot be studied by fluorescence spectroscopy. Dynamic photoelectron spectroscopy with both nanosecond and picosecond lasers has a bright prospect of developing new fields of application.

Acknowledgments

The author thanks his colleagues Dr. Yohji Achiba and Dr. Kenji Sato for their notable contributions to the development of excited-state photoelectron spectroscopy in this Institute. The author also wishes to thank Professor Saburo Nagakura, Director of this Institute, for his valuable suggestions on this manuscript, and Professor Yuan T. Lee of Lawrence Berkeley Laboratory, University of California, for his reading of the manuscript and his valuable comments during his stay as a visiting professor at the Institute for Molecular Science.

References

ACHIBA, Y., HIRAYA, A., and KIMURA, K., 1984a, *J. chem. Phys.*, **80,** 6047.

ACHIBA, Y., and KIMURA, K., 1984b, *J. chem. Soc. Japan* (in Japanese), **1984,** 1529.

ACHIBA, Y., SATO, K., and KIMURA, K., 1985, *J. chem. Phys.*, **82,** 3959.

ACHIBA, Y., SATO, K., SHINDO, Y., and KIMURA, K., 1981a, Construction of a time-of-flight electron analyzer for laser ionization photoelectron spectroscopy, *Annual Review* (Okazaki, Institute for Molecular Science), p. 105.

ACHIBA, Y., SATO, K., SHOBATAKE, K., and KIMURA, K., 1981b, Four-photon ionization photoelectron spectra of NH_3 and NO, *Annual Review* (Okazaki, Institute for Molecular Science), p. 106.

ACHIBA, Y., SATO, K., SHOBATAKE, K., and KIMURA, K., 1981c, *J. Photochem.*, **17,** 53.

ACHIBA, Y., SATO, K., SHOBATAKE, K., and KIMURA, K., 1982, *J. chem. Phys.*, **77,** 2709.

ACHIBA, Y., SATO, K., SHOBATAKE, K., and KIMURA, K., 1983a, *J. chem. Phys.*, **78,** 5474.

ACHIBA, Y., SATO, K., SHOBATAKE, K., and KIMURA, K., 1983b, *J. chem. Phys.*, **79,** 5213.

ACHIBA, Y., SHOBATAKE, K., and KIMURA, K., 1980, Construction of an apparatus for studying multiphoton ionization electron and mass spectroscopy, *Annual Review* (Okazaki, Institute for Molecular Science), p. 100.

AGOSTINI, P., CLEMENT, M., FABLRE, F., and PETITE, G., 1981, *J. Phys.* B, **14,** L491.

ANDERSON, S. L., RIDER, D. M., and ZARE, R. N., 1982, *Chem. Phys. Lett.*, **93,** 11.

ANDERSON, S. L., KUBIAK, G. D., and ZARE, R. N., 1984, *Chem. Phys. Lett.*, **105,** 22.

ANTONOV, V. S., and LETOKHOV, V. S., 1981, *Appl. Phys.*, **24,** 89.

ARON, K., OTIS, C., DEMARAY, R. E., and JOHNSON, P. M., 1980, *J. chem. Phys.*, **73,** 4167.

BARDSLEY, J. N., 1983, *Planet. Space Sci.*, **31,** 667.

BEKOV, G. I., and LETOKHOV, V. S., 1983, *Appl. Phys.* B, **30,** 161.

BERKOWITZ, J., 1979, *Photoabsorption, Photoionization, and Photoelectron Spectroscopy* (New York: Academic).

BERRY, R. S., 1976, *Electron and Photon Interactions with Atoms*, edited by H. Kleinpoppen and M. R. C. McDowell (New York, Plenum), p. 559.

CALLOMON, J. H., PARKIN, J. E., and LOPEZ -DELGADO, R., 1972, *Chem. Phys. Lett.*, **13,** 125.

COMPTON, R. N. MILLER, J. C., CARTER, A. E., and KRUIT, P., 1980, *Chem. Phys. Lett.*, **71,** 87.

COMPTON, R. N., STOCKDALE, J. A. D., COOPER, C. D., TANG, X., and LAMPBROPOULOS, P., 1984, *Phys. Rev.* A, **30,** 1766.

CONAWAY, W. E., MORRISON, R. J. S., and ZARE, R. N., 1985, *Chem. Phys. Lett.*, **113,** 429.

DOUGLAS, A. E., 1963, *Discuss. Faraday Soc.*, **35,** 158.

DUNCAN, M. A., DIETZ, T. G., and SMALLEY, R. E., 1979, *Chem. Phys.*, **44,** 415.

DURANT, J. L., RIDER, D. M., ANDERSON, S. L., PROCH, F. D., and ZARE, R. N., 1984, *J. chem. Phys.*, **80,** 1817.

DYKE, J. M., GRAVENOR, B. W., LEWIS, R. A., and MORRIS, A., 1982, *J. Phys.* B, **15,** 4523.

EDELSTEIN, S., LAMBROPOULOS, M., DUNCANSON, J., and BERRY, R. S., 1974, *Phys. Rev.* A, **9,** 2459.

ELAND, J. H., 1980, *J. Chim. phys.*, **77,** 613.

ENGELKING, P. C., 1980, *Chem. Phys. Lett.*, **74,** 207.

FELDMANN, D., and WELGE, K. H., 1982, *J. Phys.* B, **15,** 1651.

FISANIK, G. J., GEDANKEN, A., EICHELBERGER IV, T. S., KUEBLER, N. A., and ROBIN, M. B., 1981, *J. chem. Phys.*, **75,** 5215.

FUKE, K., YOSHIUCHI, H., KAYA, K., ACHIBA, Y., SATO, K., and KIMURA, K., 1984, *Chem. Phys. Lett.*, **108,** 179.

GEDANKEN, A., ROBIN, M. B., and KUEBLER, N. A., 1982, *J. phys. Chem.*, **86,** 4096.

GERRITY, D. P., ROTHBERG, L. J., and VAIDA, V., 1980, *Chem. Phys. Lett.*, **74,** 1.

GLOWNIA, J. H., RILEY, S. J., COLSON, S. D., and NIEMAN, G. C., 1980, *J. chem. Phys.*, **73,** 4296.

GLOWNIA, J. H., RILEY, S. J., COLSON, S. D., MILLER, J. C., and COMPTON, R. N., 1982, *J. chem. Phys.*, **77,** 68.

GOBELI, D. A., YANG, J. J., and EL-SAYED, M. A., 1984, *Advances in Multi-Photon Processes and Spectroscopy*, edited by S. H. Lin (Singapore: World Scientific), pp. 52–103.

GUISTI-SUZOR, A., and JUNGEN, CH., 1984, *J. chem. Phys.*, **80,** 986.

HACKETT, P. A., BACK, R. A., and KODA, S., 1977, *J. chem. Phys.*, **15,** 5103.

HANSEN, J. C., DUNCANSON, JR., J. A., CHIEN, R. L., and BERRY, R. S., 1980, *Phys. Rev.* A, **21,** 222.

HEPBURN, J. W., TREVOR, D. J., POLLARD, J. E., SHIRLEY, D. A., and LEE, Y. T., 1982, *J. chem. Phys.*, **76,** 4287.

HIRAYA, A., ACHIBA, Y., MIKAMI, N., and KIMURA, K., 1985, *J. chem. Phys.*, **82,** 1810.
HUBER, K. P., 1964, *Helv. Phys. Acta*, **37,** 329.
JOHNSON, P. M., 1980 a, *Accts Chem. Res.*, **13,** 20.
JOHNSON, P. M., 1980 b, *Appl. Optics*, **19,** 3920.
JOHNSON, P. M., and OTIS, C. E., 1981, *Rev. phys. Chem.*, **32,** 139.
JUNGEN, CH., 1966, *Can. J. Phys.*, **44,** 3197.
KAMINSKI, H., KESSLER, J., and KOLLARTH, K. J., 1980, *Phys. Rev. Lett.*, **45,** 1161.
KATZ, B., BRITH, M., SHARF, B., and JORTNER, J., 1970, *J. chem. Phys.*, **52,** 88.
KAWASAKI, M., KASATANI, K., SATO, H., ACHIBA, Y., SATO, K., and KIMURA, K., 1985, *Chem. Phys. Lett.*, **114,** 473.
KIMMAN, J., KRUIT, P., and VAN DER WIEL, M. J., 1982, *Chem. Phys. Lett.*, **88,** 576.
KIMURA, K., KATSUMATA, S., ACHIBA, Y., YAMAZAKI, T., and IWATA, S., 1981, *Handbook of HeI Photoelectron Spectra of Fundamental Organic Molecules* (Tokyo, New York: Japan Science Societies/Halstad).
KIMURA, K., 1985, *Adv. chem. Phys.*, **60,** 161.
KRUIT, P., KIMMAN, J., and VAN DER WIEL, M. J., 1981, *J. Phys.* B, **14,** L597.
KRUIT, P., and READ, F. H., 1983, *J. Phys.* E, **16,** 313.
LAMBROPOULOS, P., and SMITH, S. J., 1984, *Multiphoton Processes* (Berlin: Springer).
LEUTWYLER, S., and EVEN, U., 1981, *Chem. Phys. Lett.*, **84,** 188.
LEUTWYLER, S., EVEN, U., and JORTNER, J., 1980, *Chem. Phys. Lett.*, **74,** 11.
LETOKOV, V. S., 1983, *Nonlinear Laser Chemistry* (Berlin: Springer), pp. 169–180, 314–347.
LICHTIN, D. A., ZANDEE, L., and BERNSTEIN, R. B., 1981, *Lasers in Chemical Analysis*, edited by G. M. Heiftje, J. C. Travis and F. Elytle (New Jersey, Humana), p. 125.
LIN, S. H., FUJIMURA, Y., NEUSSER, H. J., and SCHLAG, E. W., 1984, *Multiphoton Spectroscopy of Molecules* (New York, Academic), pp. 67–68, 169–221.
LONG, S. R., MEEK, J. T., HARRINGTON, P. J., and REILLY, J. P., 1983, *J. chem. Phys.*, **78,** 3341.
MEEK, T., JONES, R. K., and REILLY, J. P., 1980, *J. chem. Phys.*, **73,** 3503.
MEEK, T., LONG, S. R., and REILLY, J. P., 1982, *J. phys. Chem.*, **86,** 2809.
MEEK, J. T., SEKRETA, E., WILSON, W., VISWANATHAN, K. S., and REILLY, J. P., 1986, *J. Phys. Chem.*, **82,** 1741.
MIESCHER, E., 1976, *Can. J. Phys.*, **54,** 2074.
MIESCHER, E., and ALBERTI, F., 1976, *J. Phys. Chem. Ref. Data*, **5,** 306.
MILLER, J. C., and COMPTON, R. N., 1981 a, *J. chem. Phys.*, **75,** 22.
MILLER, J. C., and COMPTON, R. N., 1981 b, *J. chem. Phys.*, **75,** 2020.
MILLER, J. C., and COMPTON, R. N., 1982, *Chem. Phys. Lett.*, **93,** 453.
MURAKAMI, J., KAYA, K., and ITO, M., 1980, *J. chem. Phys.*, **72,** 3263.
NAGANO, Y., ACHIBA, Y., SATO, K., and KIMURA, K., 1982, *Chem. Phys. Lett.*, **93,** 510.
NAGONO, Y., ACHIBA, Y., and KIMURA, K., 1986 a, *J. chem. Phys.*, **84,** 1063.
NAGANO, Y., ACHIBA, Y., and KIMURA, K., 1986 b, *J. phys. Chem.*, **90,** 615.
NAGANO, Y., ACHIBA, Y., and KIMURA, K., 1986 c, *J. phys. Chem.*, **90,** 1288.
PARKER, D. H., 1983, *Ultrasensitive Laser Spectroscopy*, edited by D. S. Kliger (New York: Academic), pp. 233–309.
PARMENTER, C. S., 1982, *J. phys. Chem.*, **86,** 1735.
PARMENTER, C. S., and SCHUYLER, M. W., 1970, *Chem. Phys. Lett.*, **6,** 339.
PRATT, S. T., POLIAKOFF, E. D., DEHMER, P. M., and DEHMER, J. L., 1983 a, *J. chem. Phys.*, **78,** 65.
PRATT, S. T., DEHMER, P. M., and DEHMER, J. L., 1983 b, *J. chem. Phys.*, **78,** 4315.
PRATT, S. T., DEHMER, J. L., and DEHMER, P. M., 1984 a, *Chem. Phys. Lett.*, **105,** 28.
PRATT, S. T., DEHMER, J. L., and DEHMER, P. M., 1984 b, *J. chem. Phys.*, **80,** 1706.
PRATT, S. T., DEHMER, J. L., and DEHMER, P. M., 1985 a, *J. chem. Phys.*, **82,** 676.
PRATT, S. T., DEHMER, J. L., and DEHMER, P. M., 1985 b, *J. chem. Phys.*, **82,** 5758.
PRATT, S. T., DEHMER, J. L., and DEHMER, P. M., 1985 c, *J. chem. Phys.*, **83,** 5380.
ROBIN, M. B., 1980, *Appl. Opt.*, **19,** 3941.
SATO, K., ACHIBA, Y., and KIMURA, K., 1984 a, *J. chem. Phys.*, **80,** 57.
SATO, K., ACHIBA, Y., and KIMURA, K., 1984 b, *J. chem. Phys.*, **81,** 57.
SATO, K., ACHIBA, Y., and KIMURA, K., 1986, *Chem. Phys. Lett.*, **126,** 306.
SCHLAG, E. W., and NEUSSER, H. J., 1983, *Accts Chem. Res.*, **16,** 355.
SELINGER, B. K., and WARE, W. R., 1970, *J. chem. Phys.*, **53,** 3160.
SMALLEY, R. E., 1983, *A. Rev. phys. Chem.*, **34,** 129.

SIEGBAHN, K., ALLISON, D. A., and ALLISON, J. H., 1974, *Handbook of Spectroscopy*, edited by J. W. Robinson (Florida, CRC), Volume 1, p. 257.

TURNER, D. W., BAKER, A. D., BAKER, C., and BRUNDLE, C. R., 1970, *Photoelectron Spectroscopy, A Handbook of He 854 A Spectra* (London: Interscience).

WHETTEN, R. L., FU, K.-J., and GRANT, E. R., 1983, *J. chem. Phys.*, **79**, 4899.

WHITE, M. G., CHUPKA, W. A., SEAVER, M., WOODWARD, A., and COLSON, S. D., 1984, *J. chem. Phys.*, **80**, 678.

WHITE, M. G., SEAVER, M., CHUPKA, W. A., and COLSON, S. D., 1982, *Phys. Rev. Lett.*, **49**, 28.

WILKINSON, P. G., 1956, *Can. J. Phys.*, **34**, 596.

YOSHIHARA, K., SUMITANI, M., O'CONNOR, D. V., TAKAGI, Y., and NAKASHIMA, N., 1984, *Ultrafast Phenomena IV*, edited by D. H. Auston and K. B. Eisenthal (Berlin: Springer), p. 345.